Journal of Sound and Vibration (1999) **228**(2), 275–303
Article No. jsvi.1999.2414, available online at http://www.idealibrary.com on IDEAL®

A LUMPED-MASS MODEL FOR THE DYNAMIC ANALYSIS OF THE SPATIAL BEAM-LIKE LATTICE GIRDERS

J.-S. Wu, M. Hsieh and C.-L. Lin

Institute of Naval Architecture and Marine Engineering, National Cheng-Kung University, Tainan, Taiwan 70101, *Republic of China*

(*Received* 6 *August* 1998, *and in final form* 12 *April* 1999)

A method is presented to replace the distributed mass of each bay of a spatial beam-like lattice girder by 24 lumped masses, half of the latter being located at the upper plane and the other half at the lower one of the bay respectively, where the correct magnitude and location of each lumped mass are determined according to the actual arrangement of all the members constituting the bay. Based on the locations of the 24 lumped masses, the coefficients associated with the "masses" translating in the $\bar{x}$, $\bar{y}$ and $\bar{z}$ directions and those associated with the "mass moment of inertias" rotating about the $\bar{x}$-, $\bar{y}$-, and $\bar{z}$-axis for the effective mass matrix of a bay-equivalent (continuum) beam are calculated. Numerical results show that the presented lumped-mass model together with the effective stiffness matrix of the bay-equivalent beam derived on the assumption that the cross-sections at both ends of each bay remain plane after deformation will give more accurate natural frequencies for the multi-bay spatial X-braced, Pratt or Warren beam-like lattice girders. Besides, the presented lumped-mass model is available for various transverse side-length ratios R_{ab} and longitudinal side-length ratios R_{aL}.

1. INTRODUCTION

Although the finite element method (FEM) is available for either the static or the dynamic analysis of a large complex structure such as the multi-bay spatial X-braced, Pratt, or Warren lattice girders, the requirements of much computer time and large storage capacity have led many researchers to devote themselves to the study of structural simplification methods. The so-called structural simplification methods presented in references [1–11] are to replace a complex beam-like structure by a simple equivalent (continuum) beam on which the static or the dynamic analysis is made. The main difference between existing structural simplification methods is the evaluation technique for the effective stiffness matrix and the effective mass matrix of the simple equivalent beam.

For the two-dimensional (planar) beam-like truss structures, Sun and his co-authors [4–7] derived the effective stiffness and mass matrices for the equivalent (continuum) beam element with the conventional FEM. The effective shear rigidity (GA), the effective bending rigidity (EI), and the effective axial rigidity (EA) of the

0022-460X/99/470275 + 29 $30.00/0

equivalent beam were determined by using a numerical test on a typical cell (or bay), and the effective mass per unit length of the equivalent beam was obtained by dividing the total mass of the typical cell by the length of the cell. This simplification method would be more useful if it is extended to the three-dimensional (spatial) frame structures. By equating the total strain energy and the total kinetic energy of the equivalent beam to those of the original two-dimensional (planar) lattice girder, Noor and Nemeth [8] determined the effective stiffness and mass matrices for the equivalent beam through the application of the micropolar continuum beam theory. Later in the same year, they extended the same approach for solving the two-dimensional lattice girders to the three-dimensional ones [9]. It appears that the last approach could be improved by developing a simplified derivation of the effective property matrices and by deriving the recovering expressions for nodal forces and nodal displacements in each constituent member of the original complex structure from the simple equivalent micropolar (continuum) representation of the beam.

Under the assumption that the cross-sections at both ends of each bay remain plane after deformation, Wu and Tsai derived the effective stiffness matrix and the effective mass matrix of the equivalent (continuum) beam of the two-dimensional (planar) lattice girder in 1993 [1] and those of the three-dimensional (spatial) lattice girder in 1994 [11]. The derivation of the effective property matrices for the simple equivalent beam and that of the recovering expressions for the nodal forces and nodal displacements in each constituent member presented in references [10, 11] are very simple, but the lumped mass model of reference [11] is suitable only for the case of transverse side-length ratio near unity (i.e. $R_{ab} \approx 1.0$). The purpose of this paper is to improve on this drawback.

During the derivation of the effective lumped mass matrix, attention should be paid to the magnitudes and locations of all the lumped masses by which the total mass of the original complex structure is replaced. Since some coefficients for the effective mass matrix are associated with the mass moment of inertias and, by definition, the moment of inertia of a lumped mass is equal to the product of its magnitude and the square of the distance between the lumped mass and the rotation axis, if a certain lumped mass is located at the rotation axis, then its contribution on the effective mass matrix is nil. For a two-dimensional lattice girder on the $\overline{xy}$-plane, one is only required to determine the moment of inertia about the $\bar{z}$-axis, but for a three-dimensional lattice girder in the $\overline{xyz}$-space one is required to determine the mass moment of inertia about the $\bar{x}$, $\bar{y}$- and $\bar{z}$-axis respectively. It is evident that the factors having to do with the determination of the latter are much more than those of the former, which is the reason why a lumped-mass model for the two-dimensional lattice girders [4–7, 10] is adequate for various cases, but a similar one for the three-dimensional lattice girders [11] is suitable only for the case of transverse side-length ratio near unity (i.e., $R_{ab} \approx 1{\cdot}0$).

In general, the accuracy of an approach depends on the degree of agreement between the assumptions and the actual situations. For the present paper, the effective stiffness matrix of the simple equivalent (continuum) beam is obtained on the assumption that the cross-sections at both ends of each bay remain plane after deformation. Now that the multi-bay spatial lattice girder is replaced by a simple equivalent "beam", the last assumption will be reasonable since it is one of the main

assumptions for a general "beam" theory. On the other hand, the effective lumped-mass matrix of the bay-equivalent beam is obtained from the lumped-mass model of a typical bay and the distribution (including the magnitudes and the locations) of all the lumped masses for the lumped-mass model is also quite close to the actual structure.

In view of the close agreement between the numerical results obtained from the presented structural simplification method (SSM) and those obtained from the conventional finite element method (FEM), it is believed that the last assumption and the mathematical model for the dynamic analysis of the spatial beam-like lattice girders should be reasonable. In other words, for a tall spatial beam-like lattice girder performing "global" (beam-like) transverse bending vibrations (rather than the vibrations including the "local" modes of the individual members), the effect of deformation due to the (horizontal) battens is negligible. According to the micropolar beam theory [8] the deformation of the battens is more concerned with the "local" modes.

2. STIFFNESS MATRIX OF THE BAY-EQUIVALENT BEAM

Figure 1 shows the three types of spatial beam-like lattice girders studied in this paper: (a) X-braced, (b) Pratt, and (c) Warren. Figure 2 shows a typical bay and its equivalent continuum beam ($\bar{c}\bar{d}$) of the X-braced lattice girder. Figure 3 shows the 12 degrees of freedom of a single member or a bay-equivalent beam [11].

If the cross-sections at both ends of each bay remain plane after deformation (i.e., the effect of deformation due to the (horizontal) battens is neglected), then from

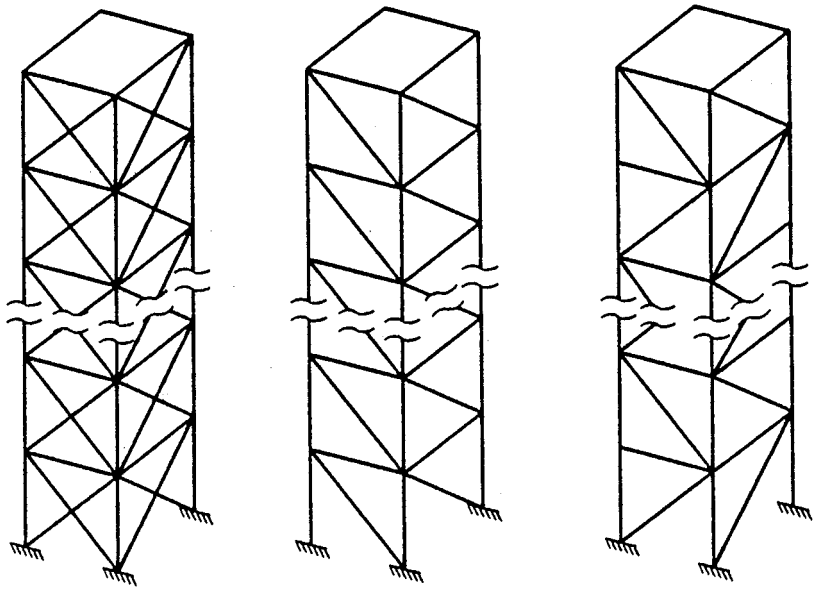

Figure 1. Three types of spatial lattice girders studied: (a) X-braced; (b) Pratt; (c) Warren.

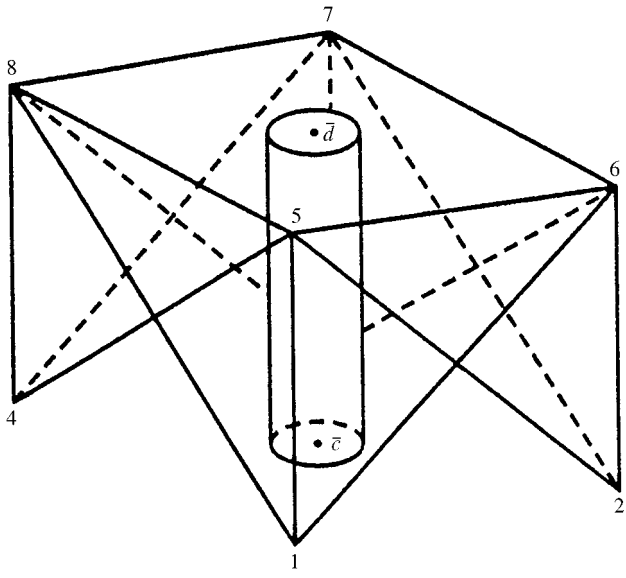

Figure 2. A typical bay and its equivalent beam of the X-braced lattice girder.

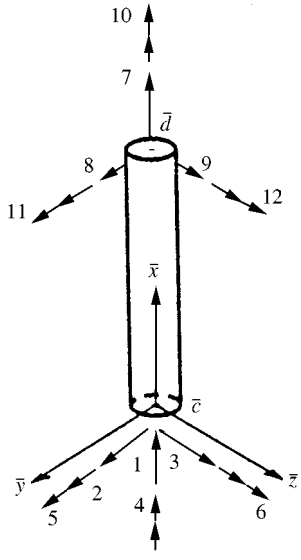

Figure 3. Degrees of freedom of a member or a bay-equivalent beam.

Figure 2, one obtains the relationship between the nodal displacement vectors $\{\delta_i\}$ at the lower section (or plane) of a bay and those at the lower end ($\bar{c}$) of its equivalent beam, $\{\delta_c\}$, to be [11]

$$\{\delta_i\} = [r_i]\{\delta_c\}, \quad i = 1\text{–}4, \tag{1}$$

where

$$\{\delta_i\} = \{u_{\bar{x}_i}\ u_{\bar{y}_i}\ u_{\bar{z}_i}\ \theta_{\bar{x}_i}\ \theta_{\bar{y}_i}\ \theta_{\bar{z}_i}\}, \tag{2}$$

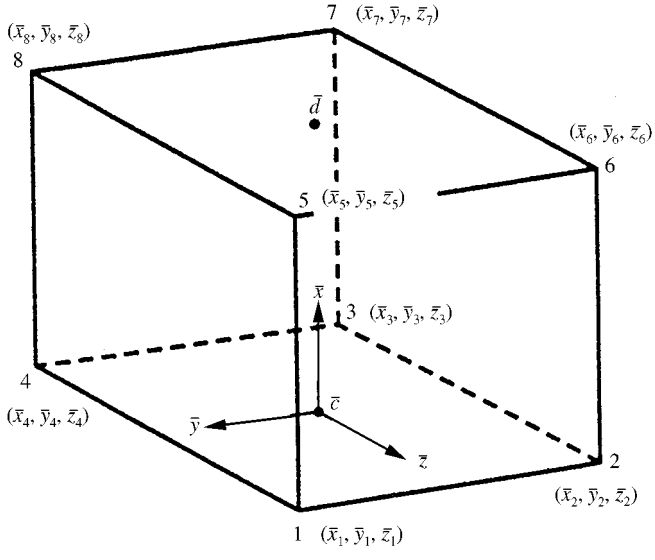

Figure 4. Nodal co-ordinates $(\bar{x}_i, \bar{y}_i, \bar{z}_i)$, $i = 1$–8, at both end cross-sections of a bay.

$$\{\delta_c\} = \{u_{\bar{x}_c}\ u_{\bar{y}_c}\ u_{\bar{z}_c}\ \theta_{\bar{x}_c}\ \theta_{\bar{y}_c}\ \theta_{\bar{z}_c}\}, \tag{3}$$

$$[r_i] = \begin{bmatrix} 1 & 0 & 0 & 0 & \bar{z}_i & -\bar{y}_i \\ 0 & 1 & 0 & -\bar{z}_i & 0 & 0 \\ 0 & 0 & 1 & \bar{y}_i & 0 & 0 \\ 0 & 0 & 0 & 1 & 0 & 0 \\ 0 & 0 & 0 & 0 & 1 & 0 \\ 0 & 0 & 0 & 0 & 0 & 1 \end{bmatrix} \tag{4}$$

and $u_{\bar{x}_i}$, $u_{\bar{y}_i}$, $u_{\bar{z}_i}$ are the translational displacements of node i in the $\bar{x}$, $\bar{y}$ and $\bar{z}$ directions respectively; $\theta_{\bar{x}_i}$, $\theta_{\bar{y}_i}$, $\theta_{\bar{z}_i}$ are the rotational angles about the $\bar{x}$, $\bar{y}$ and $\bar{z}$ axes respectively; and $\bar{y}_i$, $\bar{z}_i$ are the horizontal co-ordinate of node i with respect to the $\overline{cxyz}$ co-ordinate system as shown in Figure 4. In the foregoing equations, the symbols { } and [ ] denote the column vector and the rectangular matrix, respectively.

Similarly, for the nodal displacement vectors $\{\delta_i\}$ at the upper section (or plane) of a bay and that at the upper end $(\bar{d})$ of its equivalent beam, $\{\delta_d\}$, one has the relationship

$$\{\delta_i\} = [r_i]\{\delta_d\}, \quad i = 5\text{–}8, \tag{5}$$

where

$$\{\delta_d\} = \{u_{\bar{x}_d}\ u_{\bar{y}_d}\ u_{\bar{z}_d}\ \theta_{\bar{x}_d}\ \theta_{\bar{y}_d}\ \theta_{\bar{z}_d}\}. \tag{6}$$

From equations (1) and (5) one obtains

$$\{\delta\} = [r]\{\delta_{cd}\}, \tag{7}$$

where

$$\{\delta\} = \{\{\delta_1\}\{\delta_2\}\cdots\{\delta_8\}\}_{48\times 1}, \tag{8}$$

$$\{\delta_{cd}\} = \{\{\delta_c\}\{\delta_d\}\}_{12\times 1}, \tag{9}$$

$$[r] = \begin{bmatrix} [r_1] & 0 \\ [r_2] & 0 \\ [r_3] & 0 \\ [r_4] & 0 \\ 0 & [r_5] \\ 0 & [r_6] \\ 0 & [r_7] \\ 0 & [r_8] \end{bmatrix}_{48\times 12}. \tag{10}$$

As shown in Figure 2, if $\{F\}$ and $\{F_{cd}\}$ represent the nodal force vectors of the bay and its equivalent beam ($\bar{c}\bar{d}$) respectively, the virtual work done by $\{F\}$ and that done by $\{F_{cd}\}$ should be equal to each other, i.e.,

$$\Delta\{\delta\}^{\mathrm{T}}\{F\} = \Delta\{\delta_{cd}\}^{\mathrm{T}}\{F_{cd}\}, \tag{11}$$

where $\Delta\{\delta\}$ and $\Delta\{\delta_{cd}\}$ denote the variations of $\{\delta\}$ and $\{\delta_{cd}\}$ respectively.

Let $[K_D]$ and $[K_B]$ be the stiffness matrices of the bay and its equivalent beam ($\bar{c}\bar{d}$) respectively. Then the satisfaction of Hooke's law requires that

$$\{F\} = [K_D]\{\delta\}, \tag{12}$$

$$\{F_{cd}\} = [K_B]\{\delta_{cd}\}. \tag{13}$$

The substitution of equations (7), (12) and (13) into equation (11) will lead to

$$[K_B]_{12\times 12} = [r]^{\mathrm{T}}_{12\times 48}[K_D]_{48\times 48}[r]_{48\times 12}. \tag{14}$$

The above equation defines the relationship between the stiffness matrix of a bay $[K_D]$, and that of its equivalent beam $[K_B]$. In other words, once the stiffness matrix of a bay $[K_D]$ is determined by using the conventional FEM, then that of its equivalent beam $[K_B]$ may be obtained from equation (14).

3. DERIVATION OF LUMPED-MASS MODELS AND THE ASSOCIATED MASS MATRICES

The derivation of the lumped-mass model for a typical bay is completed in two steps. In the first step, each constituent member (or beam) of the bay is divided into two equal parts and then the distributed mass of each part of the member is

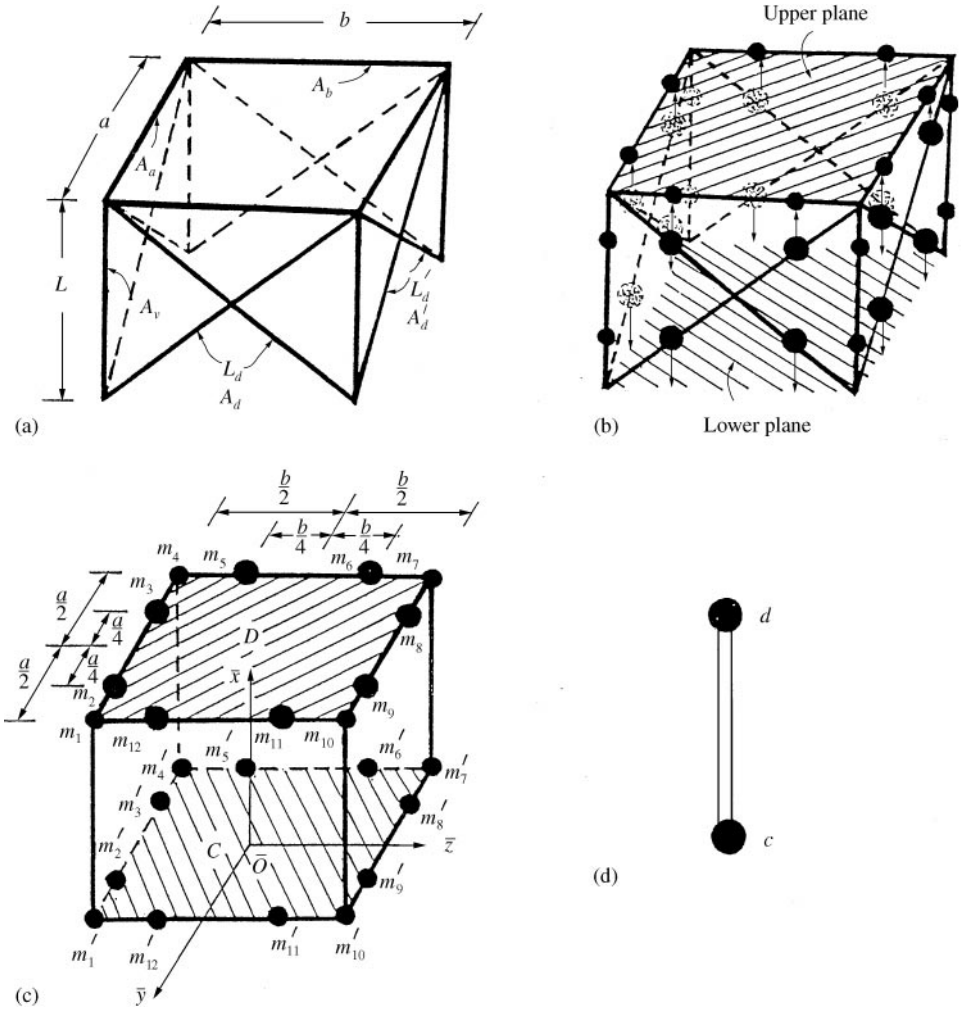

Figure 5. Derivation of lumped-mass model for the X-braced lattice girder: (a) a typical bay and its dimensions; (b) the "initial" bay lumped-mass model and the "initial" distribution of lumped masses; (c) the "final" bay lumped-mass model and the "final" distribution of lumped masses; (d) the lumped-mass model for the bay-equivalent (continuum) beam element.

replaced by a lumped mass located at the actual center of gravity (c.g.) of that part, the latter being called the "initial position" of that lumped mass. In the second step, all the lumped masses are moved from their "initial positions" to the "final positions" according to the following rules (see Figure 5):

(i) For a lumped mass on a horizontal member, its final position coincides with its initial position, and thus no movement is required.

(ii) For a lumped mass on a vertical member or on a diagonal member, it will be moved to the vertical projection of its initial position on the upper plane (or section) of the bay if it is located on the upper part of the member, and to that on the lower plane (or section) if it is located on the lower part of the member.

3.1. THE X-BRACED GIRDER

Figure 5(a) shows a typical bay of the X-braced lattice girder shown in Figure 1(a), where a and b are the lengths of horizontal members (or beams), L_d and L'_d are the lengths of the diagonal beams, and L is the length of the vertical beams. The corresponding cross-sectional areas of the above-mentioned members (or beams) are denoted by A_a, A_b, A_d, A'_d, and A_v, respectively. Figure 5(b) represents the "initial" lumped-mass model of the bay, where the magnitude of a lumped mass is approximately represented by the size of a black dot, and the directions of movement for the lumped masses on the diagonal members are shown by the upward arrows (to the upper plane) and by the downward arrows (to the lower plane). Figures 5(c) and (d) are the "final" lumped-mass model of the bay and its equivalent continuum beam respectively.

The effective lumped-mass matrix $[\bar{m}]$ of the bay-equivalent continuum beam as shown in Figure 5(d) takes the form

$$[\bar{m}] = \lceil\, [\bar{m}]_d [\bar{m}]_c \,\rfloor, \tag{15}$$

$$[\bar{m}]_d = \lceil\, m_{\bar{x}} \;\; m_{\bar{y}} \;\; m_{\bar{z}} \;\; J_{\bar{x}} \;\; J_{\bar{y}} \;\; J_{\bar{z}} \,\rfloor, \tag{16a}$$

$$[\bar{m}]_c = \lceil\, m'_{\bar{x}} \;\; m'_{\bar{y}} \;\; m'_{\bar{z}} \;\; J'_{\bar{x}} \;\; J'_{\bar{y}} \;\; J'_{\bar{z}} \,\rfloor, \tag{16b}$$

where the symbols [ ] and $\lceil \;\; \rfloor$ represent the square and diagonal matrices respectively, and the coefficients of the mass matrix are determined from Figure 5(c):

$$m_{\bar{x}} = m_{\bar{y}} = m_{\bar{z}} = \sum_{i=1}^{12} m_i, \tag{17a}$$

$$m'_{\bar{x}} = m'_{\bar{y}} = m'_{\bar{z}} = \sum_{i=1}^{12} m'_i, \tag{17b}$$

$$J_{\bar{y}} = \sum_{i=1}^{12} m_i \bar{z}_i^2 = (m_1 + m_2 + m_3 + m_4 + m_7 + m_8 + m_9 + m_{10})\left(\frac{b}{2}\right)^2 + (m_5 + m_6 + m_{11} + m_{12})\left(\frac{b}{4}\right)^2, \tag{18a}$$

$$J_{\bar{z}} = \sum_{i=1}^{12} m_i \bar{y}_i^2 = (m_1 + m_4 + m_5 + m_6 + m_7 + m_{10} + m_{11} + m_{12})\left(\frac{a}{2}\right)^2 + (m_2 + m_3 + m_8 + m_9)\left(\frac{a}{4}\right)^2, \tag{19a}$$

$$J_{\bar{x}} = J_{\bar{y}} + J_{\bar{z}}, \tag{20a}$$

$$J'_{\bar{y}} = \sum_{i=1}^{12} m'_i \bar{z}_i^2 = (m'_1 + m'_2 + m'_3 + m'_4 + m'_7 + m'_8 + m'_9 + m'_{10})\left(\frac{b}{2}\right)^2 + (m'_5 + m'_6 + m'_{11} + m'_{12})\left(\frac{b}{4}\right)^2, \tag{18b}$$

$$J'_{\bar{z}} = \sum_{i=1}^{12} m'_i \bar{y}_i^2 = (m'_1 + m'_4 + m'_5 + m'_6 + m'_7 + m'_{10} + m'_{11} + m'_{12})\left(\frac{a}{2}\right)^2 + (m'_2 + m'_3 + m'_8 + m'_9)\left(\frac{a}{4}\right)^2, \tag{19b}$$

$$J'_{\bar{x}} = J'_{\bar{y}} + J'_{\bar{z}}, \tag{20b}$$

where m_i $(i = 1\text{–}12)$ represent the lumped masses located on the upper (cross-sectional) plane D and m'_i $(i = 1\text{–}12)$ represent those located on the lower one C (see Figure 5(c)).

If the mass density and the cross-sectional area of each member composed of the bay are the same and represented by ρ and A respectively, i.e., $\rho_a = \rho_b = \rho_d = \rho'_d = \rho_v = \rho$, and $A_a = A_b = A_d = A'_d = A_v = A$, then the concentrated (lumped) masses m_i and m'_i $(i = 1\text{–}12)$ as shown in Figure 5(c) are determined by

$$\begin{aligned}
&m_i = m'_i = \tfrac{1}{2}\rho AL \quad (i = 1, 4, 7, 10),\\
&\left.\begin{aligned} m_i &= \tfrac{1}{2}\rho Aa + \tfrac{1}{2}\rho AL'_d = \tfrac{1}{2}\rho A(a + L'_d)\\ m'_i &= \tfrac{1}{2}\rho AL'_d \end{aligned}\right\} \quad (i = 2, 3, 8, 9),\\
&\left.\begin{aligned} m_i &= \tfrac{1}{2}\rho Ab + \tfrac{1}{2}\rho AL_d = \tfrac{1}{2}\rho A(b + L_d)\\ m'_i &= \tfrac{1}{2}\rho AL_d \end{aligned}\right\} \quad (i = 5, 6, 11, 12),
\end{aligned} \tag{21}$$

To substitute equation (21) into equations (17)–(20) will determine the coefficients of the lumped mass matrix $[\bar{m}]$ defined by equations (15) and (16) for the X-braced bay-equivalent beam as shown in Figure 5(d):

$$m_{\bar{x}} = m_{\bar{y}} = m_{\bar{z}} = \sum_{i=1}^{12} m_i = \tfrac{1}{2}\rho A \times 4(a + b + L + L_d + L'_d). \tag{22a}$$

$$m'_{\bar{x}} = m'_{\bar{y}} = m'_{\bar{z}} = \sum_{i=1}^{12} m'_i = \tfrac{1}{2}\rho A \times 4(L + L_d + L'_d), \tag{22b}$$

$$J_{\bar{y}} = \sum_{i=1}^{12} m_i \bar{z}_i^2 = \tfrac{1}{2}\rho Ab^2\left[(a + L + L'_d) + \tfrac{1}{4}(b + L_d)\right], \tag{23a}$$

$$J_{\bar{z}} = \sum_{i=1}^{12} m_i \bar{y}_i^2 = \tfrac{1}{2}\rho Aa^2\left[(b + L + L_d) + \tfrac{1}{4}(a + L'_d)\right], \tag{24a}$$

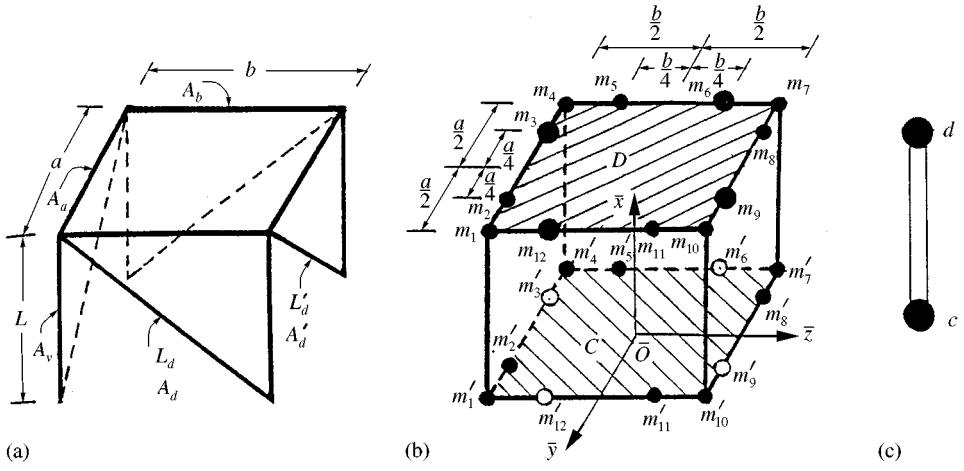

Figure 6. Derivation of lumped mass model for the Pratt lattice girder: (a) a typical bay and the associated dimensions; (b) the "final" bay lumped-mass model and the "final" distribution of lumped masses; (c) the lumped-mass model for the bay-equivalent (continuum) beam element.

$$J_{\bar{x}} = J_{\bar{y}} + J_{\bar{z}}, \tag{25a}$$

$$J'_{\bar{y}} = \sum_{i=1}^{12} m'_i \bar{z}_i^2 = \tfrac{1}{2}\rho A b^2 [(L + L'_d) + \tfrac{1}{4}L_d], \tag{23b}$$

$$J'_{\bar{z}} = \sum_{i=1}^{12} m'_i \bar{y}_i^2 = \tfrac{1}{2}\rho A a^2 [(L + L_d) + \tfrac{1}{4}L'_d], \tag{24b}$$

$$J'_{\bar{x}} = J'_{\bar{y}} + J'_{\bar{z}}. \tag{25b}$$

3.2. THE PRATT GIRDER

Except for the omission of the "initial" bay lumped-mass model together with the "initial" distribution of the lumped masses, Figures 6(a), (b) and (c) for the Pratt lattice girder are similar to Figures 5(a), (c) and (d) for the X-braced one respectively. For the case of $A_a = A_b = A_d = A'_d = A_v = A$, the lumped masses m_i ($i = 1$–12) on the upper (cross-section) plane D and those m'_i ($i = 1$–12) on the lower one C as shown in Figure 6(b) are given by

$$m_i = m'_i = \tfrac{1}{2}\rho AL \quad i = (1, 4, 7, 10),$$

$$\left.\begin{aligned} m_i &= \tfrac{1}{2}\rho Aa \\ m'_i &= \tfrac{1}{2}\rho AL'_d \end{aligned}\right\} \quad (i = 2, 8),$$

$$\left.\begin{aligned} m_i &= \tfrac{1}{2}\rho Aa + \tfrac{1}{2}\rho AL'_d \\ m_i &= 0 \end{aligned}\right\} \quad (i = 3, 9),$$

$$\left.\begin{aligned} m_i &= \tfrac{1}{2}\rho A b \\ m_i' &= \tfrac{1}{2}\rho A L_d \end{aligned}\right\} \quad (i = 5, 11),$$

$$\left.\begin{aligned} m_i &= \tfrac{1}{2}\rho A b + \tfrac{1}{2}\rho A L_d \\ m_i' &= 0 \end{aligned}\right\} \quad (i = 6, 12). \tag{26}$$

It is noted that the lumped masses represented by the small hollow circles as shown in Figure 6(b), m_i' ($i = 3, 6, 9, 12$), are zero according to the mass-distribution rules presented at the beginning of this section.

The effective lumped-mass matrix $[\bar{m}]$ for the bay-equivalent continuum beam as shown in Figure 6(c) takes the same form as that defined by equations (15) and (16). The substitution of equation (26) into equations (17)–(20) will give the coefficients of $[\bar{m}]$:

$$m_{\bar{x}} = m_{\bar{y}} = m_{\bar{z}} = \sum_{i=1}^{12} m_i = \tfrac{1}{2}\rho A[4(a + b + L) + 2(L_d + L_d')], \tag{27a}$$

$$m_{\bar{x}}' = m_{\bar{y}}' = m_{\bar{z}}' = \sum_{i=1}^{12} m_i' = \tfrac{1}{2}\rho A[4L + 2(L_d + L_d')], \tag{27b}$$

$$J_{\bar{y}} = \sum_{i=1}^{12} m_i \bar{z}_i^2 = \tfrac{1}{2}\rho A b^2 \left[\left(a + \frac{b}{4} + L\right) + (\tfrac{1}{8}L_d + \tfrac{1}{2}L_d')\right], \tag{28a}$$

$$J_{\bar{z}} = \sum_{i=1}^{12} m_i \bar{y}_i^2 = \tfrac{1}{2}\rho A a^2 \left[\left(\frac{a}{4} + b + L\right) + (\tfrac{1}{2}L_d + \tfrac{1}{8}L_d')\right], \tag{29a}$$

$$J_{\bar{x}} = J_{\bar{y}} + J_{\bar{z}}, \tag{30a}$$

$$J_{\bar{y}}' = \sum_{i=1}^{12} m_i' \bar{z}_i^2 = \tfrac{1}{2}\rho A b^2 [L + \tfrac{1}{8}L_d + \tfrac{1}{2}L_d'], \tag{28b}$$

$$J_{\bar{z}}' = \sum_{i=1}^{12} m_i' \bar{y}_i^2 = \tfrac{1}{2}\rho A a^2 (L + \tfrac{1}{2}L_d + \tfrac{1}{8}L_d'), \tag{29b}$$

$$J_{\bar{x}}' = J_{\bar{y}}' + J_{\bar{z}}'. \tag{30b}$$

3.3. THE WARREN GIRDER

The Warren lattice girder (see Figure 1(c)) is composed of two kinds of bays, the only difference between them being the directions of the diagonal beams. The lumped-mass model of one of them is the same as that of the Pratt lattice girder (see Figure 1(b)) and has been derived in the last subsection (see Figure 6), and that of the other kind of bay will be derived here. Figure 7(a) shows a typical bay and the associated dimensions, Figure 7(b) the "final" lumped-mass model and distribution, and Figure 7(c) the lumped-mass model of the equivalent (continuum) beam. For

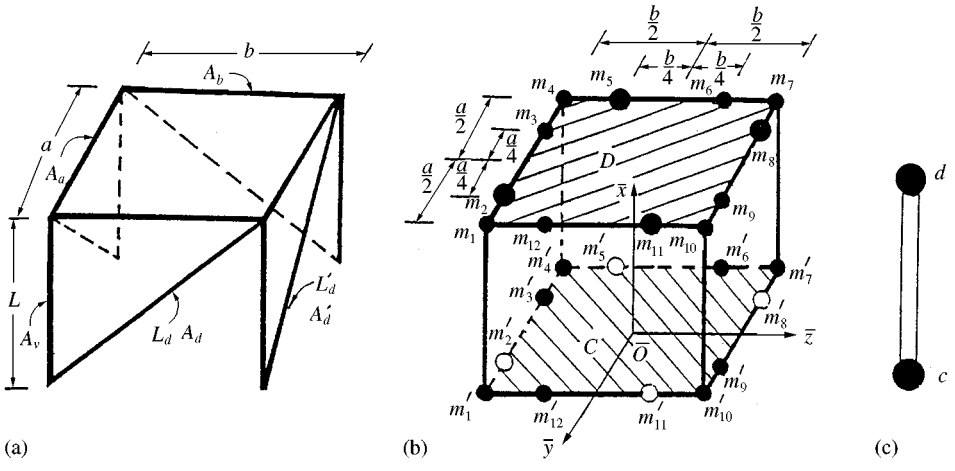

Figure 7. Derivation of lumped-mass model for one kind of bay of the Warren lattice girder: (a) a typical bay and the associated dimensions; (b) the "final" lumped-mass model and distribution; (c) the lumped-mass model of the bay-equivalent (continuum) beam element.

the cases of $A_a = A_b = A_d = A'_d = A_v = A$, from Figures 7(a) and (b) one obtains the following lumped masses:

$$m_i = m'_i = \tfrac{1}{2}\rho AL, \quad (i = 1, 4, 7, 10),$$

$$\left.\begin{aligned} m_i &= \tfrac{1}{2}\rho Aa + \tfrac{1}{2}\rho AL'_d \\ m'_i &= 0 \end{aligned}\right\} \quad (i = 2, 8),$$

$$\left.\begin{aligned} m_i &= \tfrac{1}{2}\rho Aa \\ m'_i &= \tfrac{1}{2}\rho AL'_d \end{aligned}\right\} \quad (i = 3, 9),$$

$$\left.\begin{aligned} m_i &= \tfrac{1}{2}\rho Ab + \tfrac{1}{2}\rho AL_d \\ m'_i &= 0 \end{aligned}\right\} \quad (i = 5, 11),$$

$$\left.\begin{aligned} m_i &= \tfrac{1}{2}\rho Ab \\ m'_i &= \tfrac{1}{2}\rho AL_d \end{aligned}\right\} \quad (i = 6, 12). \tag{31}$$

Similarly, the effective lumped mass matrix $[\bar{m}]$ for the bay-equivalent beam as shown in Figure 7(c) takes the same form as that defined by equations (15) and (16). The coefficients of $[\bar{m}]$ are determined by substituting equation (31) into equations (17)–(20):

$$m_{\bar{x}} = m_{\bar{y}} = m_{\bar{z}} = \sum_{i=1}^{12} m_i = \tfrac{1}{2}\rho A[4(a + b + L) + 2(L_d + L'_d)], \tag{32a}$$

$$m'_{\bar{x}} = m'_{\bar{y}} = m'_{\bar{z}} = \sum_{i=1}^{12} m'_i = \tfrac{1}{2}\rho A[4L + 2(L_d + L'_d)], \tag{32b}$$

$$J_{\bar{y}} = \sum_{i=1}^{12} m_i \bar{z}_i^2 = \tfrac{1}{2}\rho A b^2 \left[\left(a + \frac{b}{4} + L\right) + (\tfrac{1}{8}L_d + \tfrac{1}{2}L'_d)\right], \tag{33a}$$

$$J_{\bar{z}} = \sum_{i=1}^{12} m_i \bar{y}_i^2 = \tfrac{1}{2}\rho A a^2 \left[\left(\frac{a}{4} + b + L\right) + (\tfrac{1}{2}L_d + \tfrac{1}{8}L'_d)\right], \tag{34a}$$

$$J_{\bar{x}} = J_{\bar{y}} + J_{\bar{z}}, \tag{35a}$$

$$J'_{\bar{y}} = \sum_{i=1}^{12} m'_i \bar{z}_i^2 = \tfrac{1}{2}\rho A b^2 [L + \tfrac{1}{8}L_d + \tfrac{1}{2}L'_d], \tag{33b}$$

$$J'_{\bar{z}} = \sum_{i=1}^{12} m'_i \bar{y}_i^2 = \tfrac{1}{2}\rho A a^2 (L + \tfrac{1}{2}L_d + \tfrac{1}{8}L'_d), \tag{34b}$$

$$J'_{\bar{x}} = J'_{\bar{y}} + J'_{\bar{z}}. \tag{35b}$$

In the above derivations, it is assumed that $A_a = A_b = A_d = A'_d = A_v = A$. For the case of the cross-sectional areas A_a, A_b, A_d, A'_d and A_v to be not equal to each other, it is only required to replace the values of aA, bA, L_dA, L'_dA and LA by aA_a, bA_b, L_dA_d, $L'_dA'_d$ and LA_v respectively, in the above equations.

4. FREE VIBRATION ANALYSIS

Once the effective element stiffness matrix $[K_B]$ defined by equation (14) and the effective element mass matrix $[\bar{m}]$ defined by equations (15) and (16) for each bay-equivalent beam element are obtained, assembling all the element stiffness matrices $[K_B]$ and all element mass matrices $[\bar{m}]$ by using the conventional FEM and imposing the boundary (support) conditions will yield the overall stiffness matrix $[\bar{K}]$ and the overall mass matrix $[\bar{M}]$ of the entire equivalent continuum beam. The natural frequencies ω_i $(i = 1 - n')$ and the corresponding mode shapes $\{u^*\}_i$ of the equivalent beam or the original spatial beam-like lattice girder may then be determined from

$$([\bar{K}] - \omega_i^2[\bar{M}]\{u^*\}_i = 0. \tag{36}$$

In this paper, the last eigenvalue equation is solved using the Jacobi method [12].

5. NUMERICAL RESULTS AND DISCUSSION

To demonstrate the availability of the presented approach, the three kinds of beam-like lattice girders shown in Figure 1 with any number of bays (n), various

transverse side-length ratio ($R_{ab} = a/b$) and various longitudinal side-length ratio ($R_{aL} = a/L$) are studied here. The given data are

$$A_a = A_b = A_d = A'_d = 1{\cdot}5 \times 10^{-5}\ \mathrm{m}^2, \quad A_v = 3{\cdot}0 \times 10^{-5}\ \mathrm{m}^2,$$

$$\rho = 2768\ \mathrm{kg/m}^3, \quad E = 6{\cdot}895 \times 10^{10}\ \mathrm{N/m}^2, \quad G = 2{\cdot}652 \times 10^{10}\ \mathrm{N/m}^2, \tag{37}$$

where ρ is the mass density, E the Young's modulus, G is the shear modulus, and A_a, A_b, A_d, A'_d, and A_v are the cross-sectional areas of the horizontal, diagonal, and vertical members with lengths a, b, L_d, L'_d, and L as shown in Figures 5(a), 6(a) and 7(a) respectively.

5.1. INFLUENCE OF TOTAL NUMBER OF BAYS (n)

For the case of $a = b = L = 0{\cdot}75$ m, $L_d = L'_d = \sqrt{a^2 + L^2} = 1{\cdot}0607$ m (or $R_{ab} = a/b = 1{\cdot}0$ and $R_{aL} = a/L = 1{\cdot}0$), the effect of total number of bays (n) on the first six natural frequencies of the X-braced, Pratt and Warren lattice girders is shown in Figure 8, where the ordinate represents the ratio of the ith natural frequency obtained from the presented structural simplification method (ω_i) to that obtained from the conventional finite element method (ω_{iFEM}), the abscissa represents the natural frequencies ω_i ($i = 1$–6), and four kinds of shaded lines represent four kinds of total number of bays ($n = 12$, 16, 20 and 24) respectively. From the figure one can see that the effect of total number of bays (n) on the first six natural frequencies is negligible, since $\omega_i/\omega_{iFEM} \approx 1{\cdot}0$ ($i = 1$–6) for $n = 12$, 16, 20, or 24.

5.2. INFLUENCE OF SIDE-LENGTH RATIOS R_{ab} AND R_{aL}

Table 1 shows the length of the horizontal beams, a and b, and that of the vertical beams L for the cases of longitudinal side-length ratios $R_{aL} = a/L = 0{\cdot}5$–$1{\cdot}5$ and transverse side-length ratios $R_{ab} = a/b = 0{\cdot}5$–$1{\cdot}5$. The lengths of the diagonal beams are determined by $L_d = \sqrt{L^2 + b^2}$ and $L'_d = \sqrt{L^2 + a^2}$, respectively. The other physical properties of the beams for the present example are the same as those shown in equation (37).

Table 2(a) shows the effect of ratios R_{ab} and R_{aL} on the accuracy of the first six natural frequencies ω_i ($i = 1$–6) of the X-braced lattice girder with 12 bays (i.e., $n = 12$) and the CPU times consumed, where FEM and SSM represent the conventional finite element method and the structural simplification method presented in this paper respectively. The percentages ($x\%$) in the parentheses of the last column of Table 2(a) are obtained from the formula $x\% = (CPU)_{SSM} \times 100\%/(CPU)_{FEM}$, where $(CPU)_{FEM}$ is the CPU time consumed by the conventional FEM and $(CPU)_{SSM}$ is that consumed by the presented SSM. The percentage difference ($y\%$) in the other parentheses of Table 2(a) is obtained from the formula: $y\% = (\omega_{iFEM} - \omega_i) \times 100\%/\omega_{iFEM}$, $i = 1$–6, where ω_{iFEM} and ω_i are the ith natural frequencies obtained from the FEM and the presented SSM respectively.

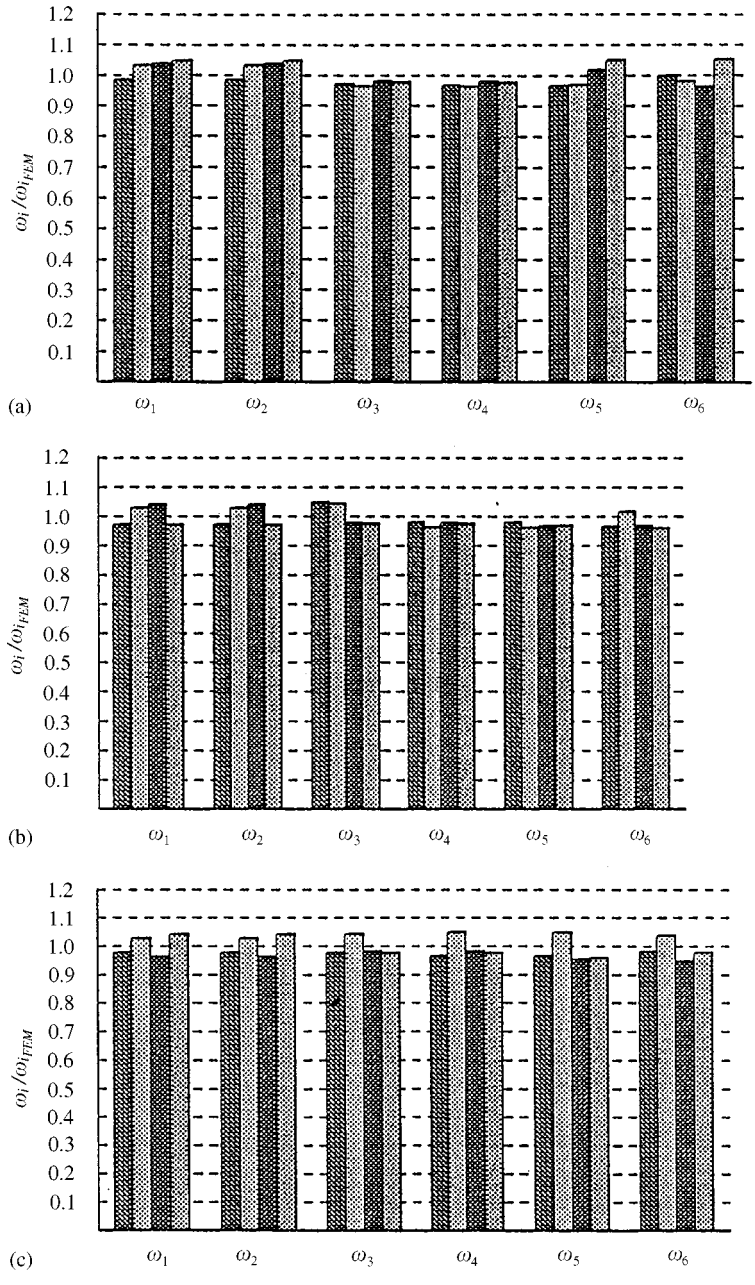

Figure 8. Effect of total number of bays (n) on the accuracy of the first six natural frequencies ω_i ($i = 1$–6) for: (a) X-braced; (b) Pratt; (c) Warren lattice girders. ■ 12 bay; ▒ 16 bay; ■ 20 bay; ▒ 24 bay.

From Table 2(a) one can see that the CPU time consumed by the presented SSM is less than 1·8% of that consumed by the conventional FEM, and the average percentage difference between the first six natural frequencies obtained from the SSM and those from the FEM is less than 2·9% for the side length ratios $R_{ab} = 0{\cdot}5$–$1{\cdot}5$ and $R_{aL} = 0{\cdot}5$–$1{\cdot}5$.

TABLE 1

Lengths of members for various side-length ratios R_{ab} and R_{aL}

$R_{aL}(=a/L)$	$R_{ab}(=a/b)$	a (m)	b (m)	L (m)
0·5	0·5	0·75	1·50	1·50
	1·0		0·75	
	1·5		0·50	
1·0	0·5	0·75	1·50	0·75
	1·0		0·75	
	1·5		0·50	
1·5	0·5	0·75	1·50	0·50
	1·0		0·75	
	1·5		0·50	

Note: $L_d = \sqrt{L^2 + b^2}$, $L'_d = \sqrt{L^2 + a^2}$.

The effect of side-length ratio R_{ab} and R_{aL} on the first six natural frequencies ω_i ($i = 1$–6) of the Pratt lattice girder is shown in Table 2(b) and that of the Warren lattice girder is shown in Table 2(c). It is evident that the conclusion just drawn from the Table 2(a) is also applicable to Tables 2(b) and (c). In other words, the effect of side-length ratios R_{ab} and R_{aL} on the accuracy of the first six natural frequencies of the X-braced, Pratt, or Warren lattice girder is negligible.

For convenience, the values R_{ab} and R_{aL} for Tables 2(a), (b) and (c) are divided into nine groups and called CASE1, CASE2, …, CASE9 respectively, as shown in Figure 9. Figures 10(a), (b), and (c) are obtained based on the data of Tables 2(a), (b), and (c) respectively. Similar to Figure 8, the ordinate of Figure 10 represents the ratio ω_i/ω_{iFEM}, abscissa represents natural frequencies ω_i ($i = 1$–6), and nine kinds of shaded lines represent the nine cases shown in Figure 9. From Figure 10 one can see that $\omega_i/\omega_{iFEM} \approx 1{\cdot}0$ ($i = 1$–6) for various side-length ratios $R_{ab} = 0{\cdot}5$–$1{\cdot}5$ and $R_{aL} = 0{\cdot}5 \sim 1{\cdot}5$.

5.3. ACCURACY OF THE HIGHER MODES

To check the accuracy of the natural frequencies of the higher modes, the values of ω_i ($i = 7$–12) for three kinds of 12-bay lattice girders obtained from the presented SSM and those determined by using the conventional finite element method (FEM) were compared. To save space, only the case of $R_{aL} = a/L = 1{\cdot}0$ and $R_{ab} = a/b = 1{\cdot}0$ is shown in Table 3. From the table one can see that the results obtained from the SSM are in close agreement with those obtained from the FEM.

5.4. THE FIRST SIX MODE SHAPES

For the 12-bay X-braced, Pratt and Warren lattice girders with $R_{aL} = a/L = 1{\cdot}0$ and $R_{ab} = a/b = 1{\cdot}0$, their first six mode shapes are shown in Tables 5–7 in

TABLE 2

The influence of ratios R_{ab} and R_{aL} on the accuracy of natural frequencies ω_i ($i = 1$–6) and the CPU times consumed for the 12*-bay lattice girder*

$R_{aL} = a/L$	$R_{ab} = a/b$		Natural frequencies (Hz) ω_1	ω_2	ω_3	ω_4	ω_5	ω_6	CPU time (s)
(a) *X-braced girder*									
		FEM	2·050	4·366	11·589	15·168	23·129	30·378	463·1
	0·5	SSM	1·957	4·291	11·513	15·426	22·538	29·309	3·8
			(4·5%)	(1·7%)	(2·9%)	(1·7%)	(3·3%)	(3·5%)	(0·8%)
		FEM	2·353	2·356	13·606	13·609	15·003	33·457	441·4
	1·0	SSM	2·281	2·284	13·068	13·229	14·742	33·051	3·6
0·5			(3·1%)	(3·1%)	(3·9%)	(2·7%)	(1·7%)	(1·2%)	(0·8%)
		FEM	1·560	2·475	9·405	12·193	14·238	23·839	465·0
	1·5	SSM	1·639	2·386	9·202	12·488	13·659	23·348	5·1
			(−5·0%)	(3·6%)	(2·1%)	(−2·4%)	(4·0%)	(2·1%)	(1·1%)
		FEM	7·056	14·055	20·774	37·461	61·108	79·535	426·2
	0·5	SSM	6·842	13·573	20·397	37·188	58·805	76·407	3·7
			(3·0%)	(3·4%)	(1·8%)	(1·0%)	(3·7%)	(3·9%)	(0·9%)
		FEM	7·671	7·671	38·438	41·579	41·579	87·575	462·0
	1·0	SSM	7·541	7·541	37·243	40·073	40·073	87·232	3·8
1·0			(1·7%)	(1·7%)	(3·1%)	(3·7%)	(3·7%)	(0·4%)	(0·8%)
		FEM	5·361	8·320	30·434	30·747	44·948	74·760	441·7
	1·5	SSM	5·201	7·998	29·521	30·086	43·112	73·879	3·8
			(2·9%)	(3·8%)	(2·9%)	(2·1%)	(4·1%)	(1·2%)	(0·9%)
		FEM	11·763	20·073	47·207	58·372	72·362	89·701	424·7
	0·5	SSM	11·471	19·589	47·553	56·154	71·282	87·621	7·6
			(2·5%)	(2·4%)	(1·0%)	(3·8%)	(1·5%)	(2·3%)	(1·8%)
		FEM	14·720	14·720	55·139	71·407	71·407	110·050	418·3
	1·0	SSM	14·136	14·136	53·392	68·703	68·703	108·410	3·8
1·5			(3·9%)	(3·9%)	(3·1%)	(3·7%)	(3·7)	(1·5%)	(0·9%)
		FEM	10·594	15·916	42·277	57·593	78·008	121·460	438·4
	1·5	SSM	10·195	15·180	40·990	55·103	74·454	118·530	5·1
			(3·7%)	(4·6%)	(3·0%)	(4·3%)	(4·5%)	(2·4%)	(1·2%)

Appendix A. In Table 5(a) all the modal displacements are equal to zero except those in the $\bar{y}$ direction and those about the $\bar{z}$-axis. In other words, the first mode shape for the X-braced lattice girder is a bending deflection in the $\bar{y}$ direction together with the corresponding rotations of cross-sections about the $\bar{z}$-axis. For the definition of $\bar{x}$-, $\bar{y}$- and $\bar{z}$-axis, one may refer to Figures 4 and 5(c). It is exactly similar to Table 5(a) in that the second mode shape shown in Table 5(b) is a bending deflection in the $\bar{z}$ direction together with the corresponding rotations of cross-sections about the $\bar{y}$-axis. The third mode shape shown in Table 5(c) is the torsion angles about the $\bar{x}$-axis. All the foregoing mode shapes have no nodes (excluding the end supports). The 4th mode shape shown in Table 5(d) is similar to

TABLE 2
continued

$R_{aL}=a/L$	$R_{ab}=a/b$		Natural frequencies (Hz) ω_1	ω_2	ω_3	ω_4	ω_5	ω_6	CPU time (s)
(a) *Pratt girder*									
		FEM	2·188	4·213	8·212	12·076	20·184	27·986	483·8
	0·5	SSM	2·283	4·008	8·558	11·494	19·823	27·947	5·7
			(−4·3%)	(4·8%)	(−4·1%)	(4·8%)	(1·78%)	(0·1%)	(1·2%)
		FEM	2·315	2·316	9·877	12·809	12·816	30·318	475·6
	1·0	SSM	2·403	2·429	10·099	12·277	12·339	29·365	5·1
0·5			(−3·8%)	(−4·8%)	(−2·2%)	(4·1%)	(4·2%)	(3·1%)	(1·1%)
		FEM	1·580	2·355	8·227	8·997	12·920	22·095	502·0
	1·5	SSM	1·668	2·466	8·581	8·807	12·386	21·423	5·3
			(−5·0%)	(−4·7%)	(−4·3%)	(2·1%)	(4·1%)	(3·0%)	(1·1%)
		FEM	7·564	13·165	27·845	35·739	49·243	78·868	457·4
	0·5	SSM	7·230	12·763	27·965	34·006	47·867	76·588	5·1
			(4·4%)	(3·1%)	(−0·4%)	(4·8%)	(2·7%)	(2·8%)	(1·1%)
		FEM	8·032	8·032	28·791	39·078	39·078	83·712	447·0
	1·0	SSM	7·784	7·784	27·962	38·205	38·205	80·694	5·0
1·0			(3·1%)	(3·1%)	(2·8%)	(2·2%)	(2·2%)	(3·6%)	(1·1%)
		FEM	5·697	8·308	22·194	30·574	40·377	70·589	449·6
	1·5	SSM	5·533	7·923	21·202	29·060	39·661	69·035	5·3
			(2·8)%	(4·6%)	(4·4%)	(4·9%)	(1·7%)	(2·2%)	(1·2%)
		FEM	12·628	19·941	39·559	54·390	63·437	98·396	452·6
	0·5	SSM	12·544	18·981	38·192	54·690	64·016	96·749	7·7
			(0·6%)	(4·8%)	(3·4%)	(−0·5%)	(−0·9%)	(1·6%)	(1·7%)
		FEM	15·292	15·292	34·969	62·756	62·756	122·14	433·1
	1·0	SSM	14·874	14·874	33·659	65·212	65·212	118·02	6·5
1·5			(2·7%)	(2·7%)	(3·7%)	(−3·9%)	(−3·9%)	(3·4%)	(1·5%)
		FEM	11·475	16·016	32·808	55·734	70·288	129·94	465·0
	1·5	SSM	10·920	15·498	31·536	54·519	68·813	123·57	6·4
			(4·8%)	(3·2%)	(3·8%)	(2·1%)	(2·1%)	(4·9%)	(1·4%)

the 1st mode, the only difference being that the former has one node and the latter has no node. This similarity also exists between the 5th mode shape shown in Table 5(e) and the 2nd mode. The 6th mode shape shown in Table 5(f) is a zero-node axial extension in the $\bar{x}$ direction. Because the entire structure of an X-braced lattice girder is symmetrical with respect to the $\bar{x}$-, $\bar{y}$- and $\bar{z}$-axis, the foregoing first six mode shapes of the X-braced lattice girder are "uncoupled". However, this is not true for the mode shapes of the Pratt and Warren lattice girders. In other words, all the mode shapes of the Pratt or Warren lattice girder are "coupled" and are the combinations of the bending, torsion and extension components as may be seen from Tables 6 and 7.

TABLE 2
continued

$R_{aL}=a/L$	$R_{ab}=a/b$		Natural frequencies (Hz) ω_1	ω_2	ω_3	ω_4	ω_5	ω_6	CPU time (s)
(c) *Warren girder*									
		FEM	2·193	4·287	8·573	11·948	23·312	27·182	482·0
	0·5	SSM	2·087	4·119	8·826	11·471	20·629	26·892	5·6
			(4·8%)	(3·9%)	(−2·9%)	(3·9%)	(3·2%)	(1·0%)	(1·2%)
		FEM	2·324	2·325	10·212	12·750	12·757	30·267	462·5
	1·0	SSM	2·418	2·418	9·819	12·313	12·313	29·068	4·9
0·5			(−4·0%)	(−4·0%)	(3·8%)	(3·4%)	(3·4%)	(3·0%)	(1·1%)
		FEM	1·584	2·371	8·411	8·866	12·997	22·373	507·1
	1·5	SSM	1·671	2·478	8·712	8·642	12·416	21·595	5·4
			(−5·0%)	(−4·5%)	(−3·5%)	(2·5%)	(4·4%)	(3·4%)	(1·1%)
		FEM	7·669	14·393	34·461	36·986	52·057	79·711	453·3
	0·5	SSM	7·423	14·024	33·450	35·648	50·368	77·552	5·0
			(3·2%)	(2·5%)	(2·9%)	(3·6%)	(3·2%)	(2·7%)	(1·1%)
		FEM	8·155	8·155	28·212	40·611	40·611	87·662	435·2
	1·0	SSM	7·938	7·938	27·475	39·067	39·067	85·897	4·8
1·0			(2·6%)	(2·6%)	(2·9%)	(3·8%)	(3·8%)	(2·0%)	(1·1%)
		FEM	5·731	8·458	24·131	30·679	40·782	70·793	445·4
	1·5	SSM	5·512	8·147	23·593	29·818	39·894	68·486	5·1
			(3·7%)	(3·6%)	(2·2%)	(2·8%)	(2·2%)	(3·3%)	(1·2%)
		FEM	12·962	20·023	35·403	51·732	66·877	94·546	443·7
	0·5	SSM	12·728	19·557	34·514	50·125	65·186	92·305	7·4
			(1·8%)	(2·3%)	(2·5%)	(3·1%)	(2·5%)	(2·3%)	(1·7%)
		FEM	15·926	15·926	42·523	68·895	68·895	123·190	440·0
	1·0	SSM	15·295	15·295	40·992	66·729	66·729	118·51	6·6
1·5			(3·9%)	(3·9%)	(3·6%)	(3·1%)	(3·1%)	(3·8%)	(1·5%)
		FEM	11·642	16·719	36·974	57·819	73·453	131·55·	439·5
	1·5	SSM	11·233	16·237	35·766	56·445	71·097	127·89	6·6
			(3·5%)	(2·8%)	(3·2%)	(2·4%)	(3·2%)	(2·7%)	(1·5%)

For the convenience of comparison, the features of all the modes shapes were summarized in Table 4. The features of the first six mode shapes of the X-braced lattice girder are denoted by (1), (2), …, (6) and defined in rows 3–8 of the final column of Table 4. The features of the other more complicated mode shapes are denoted by (7)–(10) and defined below Table 4. Besides, in order to depict the contribution of each components to a "coupled" mode shape, the following notations are also used in Table 4: P denotes "Predominant", S denotes "Significant" F denotes "Fair", L denotes "Low", N denotes "Negligible" and 0 denotes "Zero". For example, for the first mode of the X-braced lattice girder, $u_{\bar{y}}$ and $\theta_{\bar{z}}$ are P (predominant) but $u_{\bar{x}}$, $u_{\bar{z}}$, $\theta_{\bar{x}}$ and $\theta_{\bar{y}}$ are 0 (zero). This means that the

$$R_{aL} = a/L = 0{\cdot}5,\ R_{ab} = a/b = \begin{cases} 0{\cdot}5 - - - CASE1 \\ 1{\cdot}0 - - - CASE2 \\ 1{\cdot}5 - - - CASE3 \end{cases}$$

$$R_{aL} = a/L = 1{\cdot}0,\ R_{ab} = a/b = \begin{cases} 0{\cdot}5 - - - CASE4 \\ 1{\cdot}0 - - - CASE5 \\ 1{\cdot}5 - - - CASE6 \end{cases}$$

$$R_{aL} = a/L = 1{\cdot}5,\ R_{ab} = a/b = \begin{cases} 0{\cdot}5 - - - CASE7 \\ 1{\cdot}0 - - - CASE8 \\ 1{\cdot}5 - - - CASE9 \end{cases}$$

Figure 9. The values of R_{aL} and R_{ab} for the nine cases studied.

TABLE 3

The accuracy of natural frequencies ω_i $(i = 7–12)$ *for the* 12*-bay lattice girders* (*with* $R_{aL} = a/L = 1{\cdot}0$ *and* $R_{ab} = a/b = 1{\cdot}0$)

Kinds of girder	Method	Natural frequencies (Hz)					
		ω_7	ω_8	ω_9	ω_{10}	ω_{11}	ω_{12}
X-braced	FEM	93·045	93·045	113·11	151·04	162·99	188·48
	SSM	95·402	95·402	109·21	155·26	167·06	192·76
		(−2·53%)	(−2·53%)	(3·45%)	(−2·79%)	(−2·49%)	(−2·27%)
Pratt	FEM	83·809	83·809	94·695	129·04	136·61	136·61
	SSM	85·953	85·953	90·318	133·35	139·15	139·15
		(−2·56%)	(−2·56%)	(4·62%)	(−3·34%)	(−1·86%)	(−1·86%)
Warren	FEM	85·480	85·480	94·323	140·67	142·78	157·31
	SSM	88·950	88·950	91·246	136·02	139·11	152·29
		(−4·06%)	(−4·06%)	(3·26%)	(3·31%)	(2·57%)	3·19%)

first mode shape of the X-braced girder is an "uncoupled" bending deflection in the $\bar{y}$ direction together with the corresponding rotations of cross-sections about the $\bar{z}$-axis (see the 3rd row of Table 4). On the other hand, for the 6th mode shape of the Warren lattice girder as shown in Table 7(f), the contributions of $u_{\bar{x}}$, $u_{\bar{y}}$, $u_{\bar{z}}$, $\theta_{\bar{x}}$, $\theta_{\bar{y}}$ and $\theta_{\bar{z}}$ on the 6th mode shape are S, N, N, P, N and N respectively (see the final row of Table 4). This means that the 6th mode shape is a "coupled" mode composed of the deformations of $u_{\bar{x}}$, $u_{\bar{y}}$, $u_{\bar{z}}$, $\theta_{\bar{x}}$, $\theta_{\bar{y}}$ and $\theta_{\bar{z}}$, but the contribution of $\theta_{\bar{x}}$ is the most predominant (P) and the contribution of $u_{\bar{x}}$ is significant (S).

The features of the first six mode shapes for the Pratt lattice girder obtained from Table 6 and those for the Warren lattice girder obtained from Table 7 are shown in rows 9–14 and 15–20 of Table 4 respectively. From Table 4 one can see that the first six mode shapes for the X-braced girder are uncoupled, those for the Pratt girder and the Warren girder are coupled.

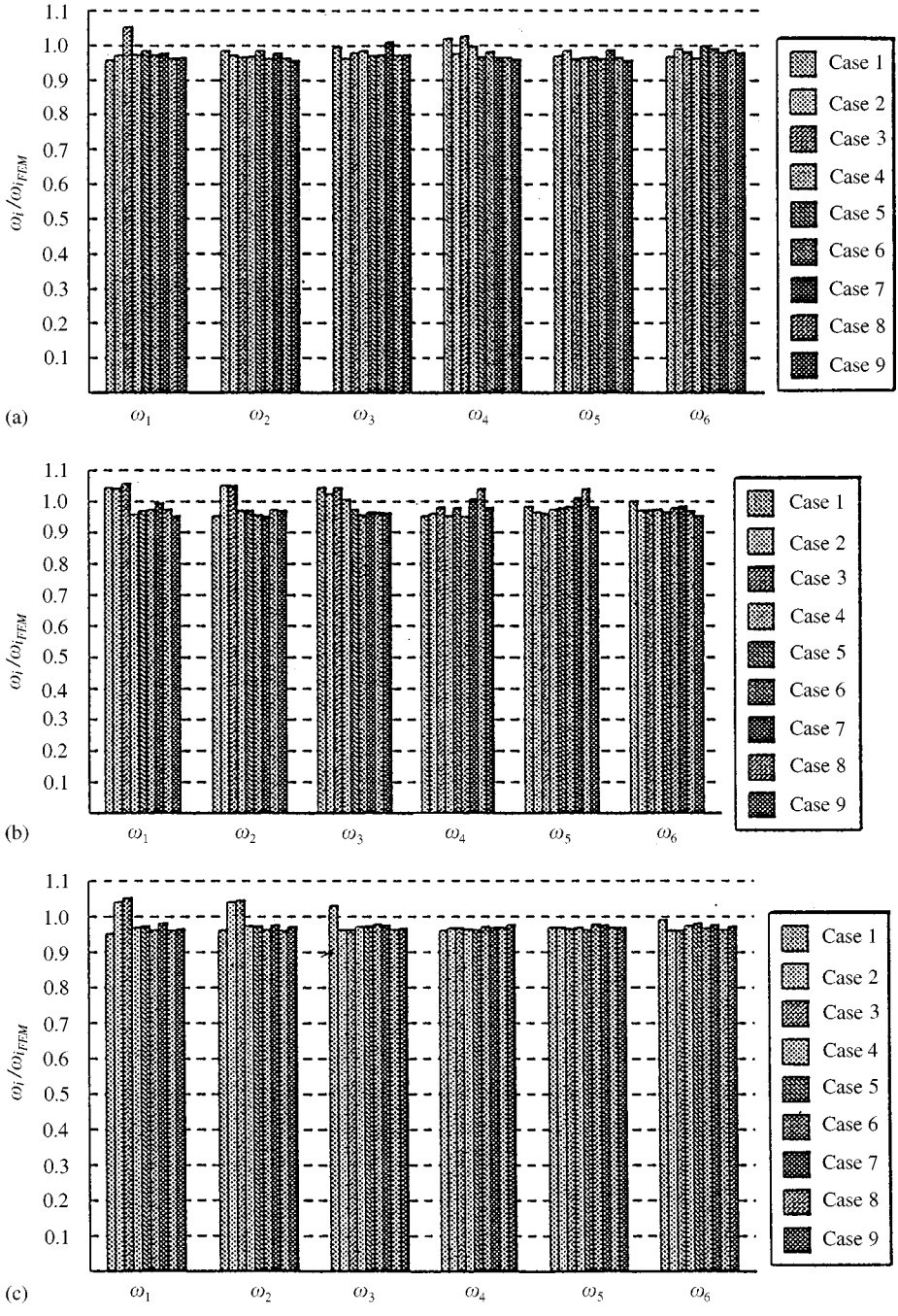

Figure 10. Influence of side-length ratios R_{ab} and R_{aL} on the accuracy of the first six natural frequencies ω_i ($i = 1$–6) for: (a) X-braced; (b) Pratt; (c) Warren lattice girder. (The values of R_{ab} and R_{aL} for each case are shown in Figure 9.)

TABLE 4

Features of the first six mode shapes for the 12-bay X-braced, Pratt and Warren lattice girders with $R_{aL} = R_{ab} = 1{\cdot}0$

Kinds of girders	Mode no.	Deformations						Descriptions
		$u_{\bar{x}}$	$u_{\bar{y}}$	$u_{\bar{z}}$	$\theta_{\bar{x}}$	$\theta_{\bar{y}}$	$\theta_{\bar{z}}$	
X-braced	1	0	*P	0	0	0	P	(1) Zero-node bending in the $\bar{y}$ direction
	2	0	0	P	0	P	0	(2) Zero-node bending in the $\bar{z}$ direction
	3	0	0	0	P	0	0	(3) Zero-node torsion aobut the $\bar{x}$ axis
	4	0	P	0	0	0	P	(4) One-node bending in the $\bar{y}$ direction
	5	0	0	P	0	P	0	(5) One-node bending in the $\bar{z}$ direction
	6	P	0	0	0	0	0	(6) Zero-node extension in the $\bar{x}$ direction
Pratt	1	N	F	P	N	P	F	(1) and (2) are coupled, but (2) is more predominant.
	2	N	P	F	N	F	P	(1) and (2) are coupled, but (1) is more predominant.
	3	F	N	N	P	N	N	(3) and (6) are coupled, but (6) is very weak.
	4	N	S	P	N	P	S	(5) and #(8) are coupled, but (5) is more predominant
	5	N	P	S	N	S	P	(4) and #(9) are coupled, but (4) is more predominant.
	6	S	N	N	P	N	N	#(7) and #(10) are coupled, but (7) is more predominant
Warren	1	N	P	S	N	F	S	(1) and (2) are coupled, but (1) is more predominant.
	2	N	S	P	N	S	L	(1) and (2) are coupled, but (2) is more predominant.
	3	L	N	N	P	N	N	(1)–(3) and (6) are coupled, but (3) is most predominant.
	4	N	P	F	N	F	P	(3)–(6) and (8) are coupled, but (4) is more predominant.
	5	N	F	P	N	P	F	(3)–(7) are coupled, but (5) is more predominant
	6	S	N	N	P	N	N	(7)–(10) are coupled, but (7) is predominant and (10) is significant.

*P: Predominant; S: Significant; F: Fair; L: Low; N: Negligible; 0: Zero. (7) One-node torsion about the $\bar{x}$ axis; (8) multi-node bending in the $\bar{y}$ direction; (9) multi-node bending in the $\bar{z}$ direction; (10) one-node extension in the $\bar{x}$ direction.

6. CONCLUSIONS

1. Compared with the conventional finite element method (FEM), the higher the total number of bays (n) that the beam-like lattice girder has, the more CPU time the presented structural simplification method (SSM) may save. The effect of the total number of bays (n) on the accuracy of the first six natural frequencies ω_i ($i = 1$–6) is negligible.
2. For a 12-bay X-braced, Pratt, or Warren lattice girder with transverse side-length ratios $R_{ab} = 0{\cdot}5$–$1{\cdot}5$ and longitudinal side-length ratios $R_{aL} = 0{\cdot}5$–$1{\cdot}5$, the maximum CPU time required by the presented SSM is less than 1·8% of that required by the conventional FEM, and the average percentage difference for the first six natural frequencies obtained from the two methods is less than 2·9%.
3. Since the entire structure of the X-braced lattice girder is symmetrical with respect to the $\bar{x}$-, $\bar{y}$- and $\bar{z}$-axis, the mode shapes are usually uncoupled. But the mode shapes of the Pratt or Warren lattice girder are the coupled ones composed of the bending, torsion and/or extension deformations.

REFERENCES

1. Z. P. Bazant and M. Christensen 1972 *International Journal of Solids Structure* **8,** 327–346. Analogy between micropolar continuum and grid frameworks under initial stress.
2. D. L. Dean and R. R. Avent 1972 *Journal Structures Division ASCE* **98**, 1903–1912. Models for approximate frame analysis.
3. C. T. Sun and T. Y. Yang 1973 *Journal of Applied Mechanics Transactions ASME* **40**, 186–192. A continuum approach toward dynamics of gridworks.
4. C. T. Sun, B. J. Kim and J. L. Bogdanoff 1981 *Proceedings AIAA/ASME 22nd Structures, Structural Dynamics and Materials Conference and AIAA Dynamics Specialists Conferences, Atlanta, GA*, 523–532. On the derivation of equivalent simple models for beam-like and plate-like structures in dynamic analysis.
5. C. C. Chen and C. T. Sun 1981 *Proceedings of the Symposium Engineering Science and Mechanics, National Cheng Kung University/American Astronautical Society*, 28–31 *December*. Transient analysis of large frame structures by simple models.
6. C. T. Sun and J. N. Juang 1986 *AIAA Journal* **24**, 144–150. Modeling global structural damping in trusses using simple continuum models.
7. B. Necib and C. T. Sun 1989 *Journal of Sound and Vibration* **130**, 149–159. Analysis of truss beams using a high order Timoshenko beam finite element.
8. A. K. Noor and M. P. Nemeth 1980 *Computations Methods in Applied Mechanics Engineering* **21**, 249–263. Micropolar beam models for lattice girds with rigid joints.
9. A. K. Noor and M. P. Nemeth 1980 *Computations Methods in Applied Mechanics Engineering* **24**, 35–59. Analysis of spatial beamlike lattices with rigid joints.
10. J. S. Wu and M. C. Tsai 1993 *Journal of Sound and Vibration* **160**, 123–136. The dynamic analysis of an X-braced lattice girder subjected to a support excitation.
11. J. S. Wu and J. M. Chen 1994 *Computers and Structures* **53**, 961–981. Dynamic analysis of spatial beam-like lattice girders.
12. K. J. Bathe and E. L. Wilson 1976 *Numerical Methods in Finite Element Analysis.* Englewood Cliffs, NJ: Prentice-Hall.

APPENDIX A: THE FIRST SIX MODE SHAPES

TABLE 5

The first six mode shapes for the 12*-bay "X-braced" girder with* $R_{aL} = R_{ab} = 1{\cdot}0$

$u_{\bar{x}}$	$u_{\bar{y}}$	$u_{\bar{z}}$	$\theta_{\bar{x}}$	$\theta_{\bar{y}}$	$\theta_{\bar{z}}$
(a) *First mode*					
0·0000E +00	0·1844E +01	0·0000E +00	0·0000E +00	0·0000E +00	0·2731E +00
0·0000E +00	0·1638E +01	0·0000E +00	0·0000E +00	0·0000E +00	0·2727E +00
0·0000E +00	0·1432E +01	0·0000E +00	0·0000E +00	0·0000E +00	0·2709E +00
0·0000E +00	0·1227E +01	0·0000E +00	0·0000E +00	0·0000E +00	0·2665E +00
0·0000E +00	0·1025E +01	0·0000E +00	0·0000E +00	0·0000E +00	0·2587E +00
0·0000E +00	0·8301E +00	0·0000E +00	0·0000E +00	0·0000E +00	0·2465E +00
0·0000E +00	0·6452E +00	0·0000E +00	0·0000E +00	0·0000E +00	0·2294E +00
0·0000E +00	0·4747E +00	0·0000E +00	0·0000E +00	0·0000E +00	0·2067E +00
0·0000E +00	0·3230E +00	0·0000E +00	0·0000E +00	0·0000E +00	0·1781E +00
0·0000E +00	0·1948E +00	0·0000E +00	0·0000E +00	0·0000E +00	0·1433E +00
0·0000E +00	0·9491E −01	0·0000E +00	0·0000E +00	0·0000E +00	0·1020E +00
0·0000E +00	0·2834E −01	0·0000E +00	0·0000E +00	0·0000E +00	0·5428E −01
0·0000E +00	0·0000E +00	0·0000E +00	0·0000E +00	0·0000E +00	0·0000E +00
(b) *Second mode*					
0·0000E +00	0·0000E +00	0·1844E +01	0·0000E +00	−0·2731E +00	0·0000E +00
0·0000E +00	0·0000E +00	0·1638E +01	0·0000E +00	−0·2727E +00	0·0000E +00
0·0000E +00	0·0000E +00	0·1432E +01	0·0000E +00	−0·2709E +00	0·0000E +00
0·0000E +00	0·0000E +00	0·1227E +01	0·0000E +00	−0·2665E +00	0·0000E +00
0·0000E +00	0·0000E +00	0·1025E +01	0·0000E +00	−0·2587E +00	0·0000E +00
0·0000E +00	0·0000E +00	0·8301E +00	0·0000E +00	−0·2465E +00	0·0000E +00
0·0000E +00	0·0000E +00	0·6452E +00	0·0000E +00	−0·2294E +00	0·0000E +00
0·0000E +00	0·0000E +00	0·4747E +00	0·0000E +00	−0·2067E +00	0·0000E +00
0·0000E +00	0·0000E +00	0·3230E +00	0·0000E +00	−0·1781E +00	0·0000E +00
0·0000E +00	0·0000E +00	0·1948E +00	0·0000E +00	−0·1433E +00	0·0000E +00
0·0000E +00	0·0000E +00	0·9491E −01	0·0000E +00	−0·1020E +00	0·0000E +00
0·0000E +00	0·0000E +00	0·2834E −01	0·0000E +00	−0·5428E −01	0·0000E +00
0·0000E +00	0·0000E +00	0·0000E +00	0·0000E +00	0·0000E +00	0·0000E +00
(c) *Third mode*					
0·0000E +00	0·0000E +00	0·0000E +00	0·1146E +01	0·0000E +00	0·0000E +00
0·0000E +00	0·0000E +00	0·0000E +00	0·1135E +01	0·0000E +00	0·0000E +00
0·0000E +00	0·0000E +00	0·0000E +00	0·1105E +01	0·0000E +00	0·0000E +00
0·0000E +00	0·0000E +00	0·0000E +00	0·1056E +01	0·0000E +00	0·0000E +00
0·0000E +00	0·0000E +00	0·0000E +00	0·9892E +00	0·0000E +00	0·0000E +00
0·0000E +00	0·0000E +00	0·0000E +00	0·9057E +00	0·0000E +00	0·0000E +00
0·0000E +00	0·0000E +00	0·0000E +00	0·8068E +00	0·0000E +00	0·0000E +00
0·0000E +00	0·0000E +00	0·0000E +00	0·6943E +00	0·0000E +00	0·0000E +00
0·0000E +00	0·0000E +00	0·0000E +00	0·5701E +00	0·0000E +00	0·0000E +00
0·0000E +00	0·0000E +00	0·0000E +00	0·4362E +00	0·0000E +00	0·0000E +00
0·0000E +00	0·0000E +00	0·0000E +00	0·2950E +00	0·0000E +00	0·0000E +00
0·0000E +00	0·0000E +00	0·0000E +00	0·1487E +00	0·0000E +00	0·0000E +00
0·0000E +00	0·0000E +00	0·0000E +00	0·0000E +00	0·0000E +00	0·0000E +00
(d) *Fourth mode*					
0·0000E +00	0·4235E +01	0·0000E +00	0·0000E +00	0·0000E +00	0·2124E +01
0·0000E +00	0·2588E +01	0·0000E +00	0·0000E +00	0·0000E +00	0·2093E +01

TABLE 5

Continued

$u_{\bar{x}}$	$u_{\bar{y}}$	$u_{\bar{z}}$	$\theta_{\bar{x}}$	$\theta_{\bar{y}}$	$\theta_{\bar{z}}$
0·0000E +00	0·9294E +00	0·0000E +00	0·0000E +00	0·0000E +00	0·1975E +01
0·0000E +00	−0·6181E +00	0·0000E +00	0·0000E +00	0·0000E +00	0·1731E +01
0·0000E +00	−0·1919E +01	0·0000E +00	0·0000E +00	0·0000E +00	0·1360E +01
0·0000E +00	−0·2853E +01	0·0000E +00	0·0000E +00	0·0000E +00	0·8887E +00
0·0000E +00	−0·3341E +01	0·0000E +00	0·0000E +00	0·0000E +00	0·3711E +00
0·0000E +00	−0·3362E +01	0·0000E +00	0·0000E +00	0·0000E +00	−0·1248E +00
0·0000E +00	−0·2958E +01	0·0000E +00	0·0000E +00	0·0000E +00	−0·5251E +00
0·0000E +00	−0·2238E +01	0·0000E +00	0·0000E +00	0·0000E +00	−0·7605E +00
0·0000E +00	−0·1365E +01	0·0000E +00	0·0000E +00	0·0000E +00	−0·7742E +00
0·0000E +00	−0·5447E +00	0·0000E +00	0·0000E +00	0·0000E +00	−0·5273E +00
0·0000E +00	0·0000E +00	0·0000E +00	0·0000E +00	0·0000E +00	0·0000E +00
(e) *Fifth mode*					
0·0000E +00	0·0000E +00	0·4235E +01	0·0000E +00	−0·2124E +01	0·0000E +00
0·0000E +00	0·0000E +00	0·2588E +01	0·0000E +00	−0·2093E +01	0·0000E +00
0·0000E +00	0·0000E +00	0·9294E +00	0·0000E +00	−0·1975E +01	0·0000E +00
0·0000E +00	0·0000E +00	−0·6181E +00	0·0000E +00	−0·1731E +01	0·0000E +00
0·0000E +00	0·0000E +00	−0·1919E +01	0·0000E +00	−0·1360E +01	0·0000E +00
0·0000E +00	0·0000E +00	−0·2853E +01	0·0000E +00	−0·8887E +00	0·0000E +00
0·0000E +00	0·0000E +00	−0·3341E +01	0·0000E +00	−0·3711E +00	0·0000E +00
0·0000E +00	0·0000E +00	−0·3362E +01	0·0000E +00	0·1248E +00	0·0000E +00
0·0000E +00	0·0000E +00	−0·2958E +01	0·0000E +00	0·5251E +00	0·0000E +00
0·0000E +00	0·0000E +00	−0·2238E +01	0·0000E +00	0·7605E +00	0·0000E +00
0·0000E +00	0·0000E +00	−0·1365E +01	0·0000E +00	0·7742E +00	0·0000E +00
0·0000E +00	0·0000E +00	−0·5447E +00	0·0000E +00	0·5273E +00	0·0000E +00
0·0000E +00	0·0000E +00	0·0000E +00	0·0000E +00	0·0000E +00	0·0000E +00
(f) *Sixth mode*					
0·1145E +01	0·0000E +00	0·0000E +00	0·0000E +00	0·0000E +00	0·0000E +00
0·1134E +01	0·0000E +00	0·0000E +00	0·0000E +00	0·0000E +00	0·0000E +00
0·1104E +01	0·0000E +00	0·0000E +00	0·0000E +00	0·0000E +00	0·0000E +00
0·1055E +01	0·0000E +00	0·0000E +00	0·0000E +00	0·0000E +00	0·0000E +00
0·9878E +00	0·0000E +00	0·0000E +00	0·0000E +00	0·0000E +00	0·0000E +00
0·9042E +00	0·0000E +00	0·0000E +00	0·0000E +00	0·0000E +00	0·0000E +00
0·8055E +00	0·0000E +00	0·0000E +00	0·0000E +00	0·0000E +00	0·0000E +00
0·6931E +00	0·0000E +00	0·0000E +00	0·0000E +00	0·0000E +00	0·0000E +00
0·5691E +00	0·0000E +00	0·0000E +00	0·0000E +00	0·0000E +00	0·0000E +00
0·4354E +00	0·0000E +00	0·0000E +00	0·0000E +00	0·0000E +00	0·0000E +00
0·2944E +00	0·0000E +00	0·0000E +00	0·0000E +00	0·0000E +00	0·0000E +00
0·1485E +00	0·0000E +00	0·0000E +00	0·0000E +00	0·0000E +00	0·0000E +00
0·0000E +00	0·0000E +00	0·0000E +00	0·0000E +00	0·0000E +00	0·0000E +00

TABLE 6

The first six mode shapes for the 12*-bay "Pratt" girder with* $R_{aL} = R_{ab} = 1{\cdot}0$

$u_{\bar{x}}$	$u_{\bar{y}}$	$u_{\bar{z}}$	$\theta_{\bar{x}}$	$\theta_{\bar{y}}$	$\theta_{\bar{z}}$
(a) *First mode*					
−0·5435E−15	0·1014E+01	0·2314E+00	−0·6299E−14	−0·3342E+00	−0·1048E−01
−0·5257E−15	0·1089E+00	0·2061E+01	−0·6837E−14	−0·3337E+00	−0·1003E−01
−0·4996E−15	0·1149E+00	0·1807E+01	−0·5681E−14	−0·3314E+00	−0·8984E−02
−0·4673E−15	0·1188E+00	0·1552E+01	−0·5266E−14	0·3259E+00	−0·7498E−02
−0·4280E−15	0·1197E+00	0·1301E+01	−0·4777E−14	−0·3163E+00	−0·5736E−02
−0·3845E−15	0·1172E+00	0·1057E+01	−0·4254E−14	0·3013E+00	−0·3867E−02
−0·3356E−15	0·1110E+00	0·8255E+00	−0·3679E−14	−0·2802E+00	−0·2052E−02
−0·2843E−15	0·1010E+00	0·6110E+00	−0·3092E−14	−0·2525E+00	−0·4483E−03
−0·2294E−15	0·8714E−01	0·4194E+00	−0·2474E−14	−0·2175E+00	0·8003E−03
−0·1734E−15	0·6972E−01	0·2564E+00	−0·1859E−14	−0·1749E+00	0·1565E−02
−0·1158E−15	0·4907E−01	0·1281E+00	−0·1233E−14	−0·1245E+00	0·1737E−02
−0·5800E−16	0·2565E−01	0·4059E−01	−0·6156E−15	−0·6625E−01	0·1234E−02
0·0000E+00	0·0000E+00	0·0000E+00	0·0000E+00	0·0000E+00	0·0000E+00
(b) *Second mode*					
−0·7451E−15	0·2380E+01	−0·1043E+00	−0·1128E−13	−0·1078E−01	0·3437E+00
−0·7363E−15	0·2120E+01	−0·1119E+00	−0·1114E−13	−0·1032E−01	0·3431E+00
−0·7130E−15	0·1858E+01	−0·1182E+00	−0·1078E−13	−0·9240E−02	0·3408E+00
−0·6761E−15	0·1596E+01	−0·1221E+00	−0·1022E−13	−0·7711E−02	0·3352E+00
−0·6269E−15	0·1338E+01	−0·1231E+00	−0·9471E−14	−0·5899E−02	0·3252E+00
−0·5673E−15	0·1087E+01	−0·1205E+00	−0·8562E−14	−0·3977E−02	0·3099E+00
−0·4990E−15	0·8490E+00	−0·1142E+00	−0·7524E−14	−0·2110E−02	0·2882E+00
−0·4240E−15	0·6284E+00	−0·1038E+00	−0·6387E−14	−0·4610E−03	0·2596E+00
−0·3440E−15	0·4313E+00	−0·8961E−01	−0·5177E−14	−0·8230E−03	0·2237E+00
−0·2605E−15	0·2637E+00	−0·7170E−01	−0·3917E−14	0·1609E−02	0·1799E+00
−0·1747E−15	0·1317E+00	−0·5047E−01	−0·2626E−14	0·1787E−02	0·1281E+00
−0·8766E−16	0·4174E−01	−0·2638E−01	−0·1317E−14	0·1269E−02	0·6813E−01
0·0000E+00	0·0000E+00	0·0000E+00	0·0000E+00	0·0000E+00	0·0000E+00
(c) *Third mode*					
0·6324E−01	0·2802E−14	0·1596E−14	0·1028E+01	−0·4934E−15	0·6138E−15
0·6261E−01	0·2303E−14	0·1230E−14	0·1018E+01	−0·4807E−15	0·6071E−15
0·6092E−01	0·1789E−14	0·8612E−15	0·9905E+00	−0·4521E−15	0·5870E−15
0·5821E−01	0·1284E−14	0·5260E−15	0·9465E+00	−0·4044E−15	0·5436E−15
0·5452E−01	0·8236E−15	0·2400E−15	0·8864E+00	−0·3414E−15	0·4772E−15
0·4991E−01	0·4317E−15	0·1741E−16	0·8114E+00	−0·2679E−15	0·3926E−15
0·4445E−01	0·1247E−15	−0·1352E−15	0·7228E+00	−0·1893E−15	0·2978E−15
0·3825E−01	−0·8975E−16	−0·2161E−15	0·6220E+00	−0·1127E−15	0·2010E−15
0·3140E−01	−0·2102E−15	−0·2305E−15	0·5106E+00	−0·4562E−16	0·1110E−15
0·2403E−01	−0·2418E−15	−0·1924E−15	0·3907E+00	0·3855E−17	−0·3683E−16
0·1625E−01	−0·1988E−15	−0·1236E−15	0·2642E+00	0·2951E−16	−0·1182E−16
0·8193E−02	−0·1064E−15	−0·5115E−16	0·1332E+00	0·2824E−16	−0·2602E−16
0·0000E+00	0·0000E+00	0·0000E+00	0·0000E+00	0·0000E+00	0·0000E+00
(d) *Fourth mode*					
−0·1862E−14	−0·3577E+00	0·6210E+01	−0·1287E−13	−0·2899E+01	−0·3654E+00
−0·1826E−14	−0·1021E+00	0·3897E+01	−0·1247E−13	−0·2862E+01	−0·3300E+00
−0·1736E−14	0·7634E−01	0·1496E+01	−0·1148E−13	0·2714E+01	−0·2553E+00

TABLE 6

Continued

$u_{\bar{x}}$	$u_{\bar{y}}$	$u_{\bar{z}}$	$\theta_{\bar{x}}$	$\theta_{\bar{y}}$	$\theta_{\bar{z}}$
−0·1605E−14	0·1315E+00	−0·7949E+00	−0·1010E−13	−0·2405E+01	−0·1619E+00
−0·1448E−14	0·5342E−01	−0·2761E+01	−0·8565E−14	−0·1929E+01	−0·7173E−01
−0·1280E−14	−0·1334E+00	−0·4212E+01	−0·7101E−14	−0·1320E+01	−0·3520E−02
−0·1110E−14	−0·3775E+00	−0·5014E+01	−0·5839E−14	−0·6456E+00	0·3073E−01
−0·9414E−15	−0·6123E+00	−0·5120E+01	−0·4800E−14	0·8403E−02	0·2863E−01
−0·7709E−15	−0·7709E+00	−0·4582E+01	−0·3910E−14	0·5460E+00	−0·1767E−02
−0·5937E−15	−0·8002E+00	−0·3545E+01	−0·3055E−14	0·8767E+00	−0·4324E−01
−0·4056E−15	−0·6731E+00	−0·2240E+01	−0·2133E−14	0·9259E+00	−0·7254E−01
−0·2063E−14	−0·3942E+00	−0·9537E+00	−0·1105E−14	0·6423E+00	−0·6503E−01
0·0000E+00	0·0000E+00	0·0000E+00	0·0000E+00	0·0000E+00	0·0000E+00
(e) *Fifth mode*					
−0·1968E−14	0·6593E+01	0·3797E+00	−0·1894E−13	−0·3879E+00	0·3078E+01
−0·1923E−14	0·4137E+01	0·1084E+00	−0·1835E−13	−0·3504E+00	0·3038E+01
−0·1810E−14	0·1588E+01	−0·8105E−01	−0·1686E−13	−0·2711E+00	0·2881E+01
−0·1643E−14	−0·8439E+00	−0·1396E+00	−0·1471E−13	−0·1719E+00	0·2553E+01
−0·1443E−14	−0·2932E+01	−0·5671E−01	−0·1222E−13	−0·7615E−01	0·2048E+01
−0·1230E−14	−0·4471E+01	0·1417E+00	−0·9715E−14	−0·3737E−02	0·1402E+01
−0·1021E−14	−0·5323E+01	0·4008E+00	−0·7435E−14	0·3262E−01	0·6854E+00
−0·8240E−15	−0·5436E+01	0·6501E+00	−0·5513E−14	0·3040E−01	−0·8921E−02
−0·6423E−15	−0·4864E+01	0·8184E+00	−0·3970E−14	−0·1876E−02	−0·5797E+00
−0·4733E−15	−0·3764E+01	0·8496E+00	−0·2743E−14	−0·4590E−01	−0·9308E+00
−0·3124E−15	−0·2378E+01	0·7146E+00	−0·1731E−14	−0·7701E−01	−0·9831E+00
−0·1444E−15	−0·1012E+01	0·4186E+00	−0·8403E−15	−0·6904E−01	−0·6819E+00
0·0000E+00	0·0000E+00	0·0000E+00	0·0000E+00	0·0000E+00	0·0000E+00
(f) *Sixth mode*					
0·1697E+00	0·1217E−14	0·2359E−14	0·2727E+01	−0·1465E−14	0·4169E−15
0·1548E+00	0·7826E−15	0·1055E−14	0·2486E+01	−0·1380E−14	0·4483E−15
0·1170E+00	0·1934E−15	−0·2501E−15	0·1872E+01	−0·1114E−14	0·4514E−15
0·6182E−01	−0·4197E−15	−0·1174E−14	0·9768E+00	−0·6740E−15	0·3555E−15
−0·2349E−02	−0·8550E−15	−0·1464E−14	−0·6467E−01	−0·1640E−15	0·1479E−15
−0·6595E−01	−0·9401E−15	−0·1101E−14	−0·1097E+01	0·2698E−15	−0·1209E−15
−0·1195E+00	−0·6250E−15	−0·2989E−15	−0·1964E+01	0·5057E−15	−0·3597E−15
−0·1549E+00	−0·2213E−16	0·5896E−15	−0·2537E+01	0·4982E−15	−0·4788E−15
−0·1669E+00	0·6268E−15	0·1216E−14	−0·2729E+01	0·2953E−15	−0·4341E−15
−0·1538E+00	0·1048E−14	0·1374E−14	−0·2512E+01	0·1745E−16	−0·2543E−15
−0·1175E+00	0·1056E−14	0·1071E−14	−0·1919E+01	−0·1909E−15	−0·3678E−16
−0·6353E−01	0·6442E−15	0·5106E−15	−0·1037E+01	−0·2142E−15	0·8643E−16
0·0000E+00	0·0000E+00	0·0000E+00	0·0000E+00	0·0000E+00	0·0000E+00

TABLE 7

The first six mode shapes for the 12*-bay "Warren" girder with* $R_{aL} = R_{ab} = 1{\cdot}0$

$u_{\bar{x}}$	$u_{\bar{y}}$	$u_{\bar{z}}$	$\theta_{\bar{x}}$	$\theta_{\bar{y}}$	$\theta_{\bar{z}}$
(a) *first mode*					
−0·1439E−15	0·2810E+01	0·6871E+00	0·8120E−14	−0·1003E+00	0·4035E+00
−0·1237E−15	0·2505E+01	0·6109E+00	0·7834E−14	−0·1007E+00	0·4028E+00
−0·1415E−15	0·2197E+01	0·5355E+00	0·7447E−14	−0·9865E−01	0·4004E+00
−0·1023E−15	0·1890E+01	0·4556E+00	0·6922E−14	−0·9919E−01	0·3934E+00
−0·1265E−15	0·1586E+01	0·3854E+00	0·6358E−14	−0·9360E−01	0·3824E+00
−0·7434E−16	0·1292E+01	0·3055E+00	0·5663E−14	−0·9249E−01	0·3636E+00
−0·1034E−15	0·1009E+01	0·2447E+00	0·4971E−14	−0·8261E−01	0·3392E+00
−0·4334E−16	0·7523E+00	0·1678E+00	0·4169E−14	−0·7849E−01	0·3047E+00
−0·7453E−16	0·5157E+00	0·1247E+00	0·3399E−14	−0·6393E−01	0·2634E+00
−0·8324E−17	0·3217E+00	0·5644E−01	0·2515E−14	−0·5588E−01	0·2109E+00
−0·3866E−16	0·1597E+00	0·3849E−01	0·1717E−14	−0·3654E−01	0·1510E+00
−0·2934E−16	0·5808E−01	−0·1457E−01	0·8099E−15	−0·2405E−01	0·7924E−01
−0·0000E+00	0·0000E+00	0·0000E+00	0·0000E+00	0·0000E+00	0·0000E+00
(b) *Second mode*					
0·2967E−15	0·6976E+00	−0·2853E+01	−0·4175E−14	0·4097E+00	0·1018E+00
0·3047E−15	0·6202E+00	−0·2543E+01	−0·4340E−14	0·4089E+00	0·1022E+00
0·2964E−15	0·5437E+00	−0·2231E+01	−0·4383E−14	0·4065E+00	0·1002E+00
0·2800E−15	0·4636E+00	−0·1919E+01	−0·4283E−14	0·3994E+00	0·1007E+00
0·2736E−15	0·3913E+00	−0·1610E+01	−0·4116E−14	0·3883E+00	0·9503E−01
0·2339E−15	0·3101E+00	−0·1312E+01	−0·3779E−14	0·3692E+00	0·9390E−01
0·2271E−15	0·2485E+00	−0·1025E+01	−0·3452E−14	0·3444E+00	0·8387E−01
0·1678E−15	0·1704E+00	−0·7637E+00	−0·2913E−14	0·3093E+00	0·7969E−01
0·1605E−15	0·1266E+00	−0·5236E+00	−0·2477E−14	0·2674E+00	0·6490E−01
0·8931E−16	0·5730E−01	−0·3266E+00	−0·1811E−14	0·2141E+00	0·5674E−01
0·8305E−16	0·3908E−01	−0·1621E+00	−0·1302E−14	0·1533E+00	0·3710E−01
0·4956E−17	−0·1479E−01	−0·5897E−01	−0·5470E−15	0·8045E−01	0·2442E+01
0·0000E+00	0·0000E+00	0·0000E+00	0·0000E+00	0·0000E+00	0·0000E+00
(c) *Third mode*					
0·4489E−02	−0·1027E−14	−0·4817E−15	0·1087E+01	−0·1105E−15	−0·1842E−15
0·5092E−02	−0·8910E−15	−0·5613E−15	0·1077E+01	−0·1085E−15	−0·1808E−15
0·3449E−02	−0·7858E−15	−0·6566E−15	0·1048E+01	−0·9111E−16	−0·1752E−15
0·6054E−02	−0·6211E−15	−0·7313E−15	0·1001E+01	−0·5964E−16	−0·1733E−15
0·2451E−02	−0·5384E−15	−0·7672E−15	0·9375E+00	−0·1684E−16	−0·1632E−15
0·6881E−02	−0·3781E−15	−0·7560E−15	0·8583E+00	0·2880E−16	−0·1491E−15
0·1558E−02	−0·3147E−15	−0·7068E−15	0·7644E+00	0·7262E−16	−0·1351E−15
0·7514E−02	−0·1928E−15	−0·6075E−15	0·6579E+00	0·1053E−15	−0·1098E−15
0·8265E−03	−0·1473E−15	−0·5002E−15	0·5400E+00	0·1279E−15	−0·9353E−16
0·7905E−02	−0·7791E−16	−0·3514E−15	0·4134E+00	0·1311E−15	−0·6204E−16
0·2979E−03	−0·4410E−16	−0·2226E−15	0·2794E+00	0·1150E−15	−0·4824E−16
0·8020E−02	−0·2964E−16	−0·8270E−16	0·1411E+00	0·7271E−16	−0·1169E−16
0·0000E+00	0·0000E+00	0·0000E+00	0·0000E+00	0·0000E+00	0·0000E−00
(d) *Fourth mode*					
−0·1479E−15	0·4409E+01	−0·1111E−01	0·2434E−14	0·1594E−01	0·2066E+01
−0·1360E−15	0·2764E+01	−0·1716E−01	0·2233E−14	−0·6925E−02	0·2039E+01
−0·1622E−15	0·1062E+01	0·3315E−01	0·1748E−14	0·3880E−01	0·1934E+01

TABLE 7

Continued

$u_{\bar{x}}$	$u_{\bar{y}}$	$u_{\bar{z}}$	$\theta_{\bar{x}}$	$\theta_{\bar{y}}$	$\theta_{\bar{z}}$
−0·1233E−15	−0·5626E+00	−0·3609E−01	−0·1103E−14	−0·1678E−01	0·1718E+01
−0·1566E−15	−0·1959E+01	0·8921E−01	0·4442E−15	0·3280E−01	0·1387E+01
−0·1177E−15	−0·2997E+01	−0·5251E−01	−0·1394E−15	−0·1419E−02	0·9631E+00
−0·1307E−15	−0·3582E+01	0·1171E+00	−0·5159E−15	0·7286E−02	0·4932E+00
−0·1076E−15	−0·3680E+01	−0·3708E−01	−0·7326E−15	0·3031E−01	0·3466E−01
−0·9131E−16	−0·3321E+01	0·9915E−01	−0·6852E−15	−0·1912E−01	−0·3441E+00
−0·7991E−16	−0·2598E+01	0·2459E−01	−0·6033E−15	0·6723E−01	−0·5844E+00
−0·4808E−16	−0·1672E+01	0·4767E−01	−0·3637E−15	−0·2617E−01	−0·6274E+00
−0·3465E−16	−0·7270E+00	0·1334E+00	−0·2492E−15	0·1038E+00	−0·4427E+00
0·0000E+00	0·0000E+00	0·0000E+00	0·0000E+00	0·0000E+00	0·0000E+00
(e) *Fifth mode*					
−0·1291E−14	0·1081E−01	0·4290E+01	−0·3894E−14	−0·2010E+01	0·1551E−01
−0·1270E−14	0·1669E−01	0·2690E+01	−0·3992E−14	−0·1984E+01	−0·6738E−02
−0·1229E−14	−0·3226E−01	0·1033E+01	−0·4019E−14	−0·1882E+01	0·3775E−01
−0·1131E−14	0·3512E−01	−0·5474E+00	−0·4605E−14	−0·1672E+01	−0·1632E−01
−0·1055E−14	−0·8680E−01	−0·1906E+01	−0·4730E−14	−0·1349E+01	0·3192E−01
−0·9216E−15	0·5109E−01	−0·2916E+01	−0·5361E−14	−0·9371E+00	−0·1380E−02
−0·7970E−15	−0·1140E+00	−0·3485E+01	−0·5042E−14	−0·4799E+00	0·7089E−02
−0·6770E−15	0·3607E−01	−0·3580E+01	−0·5203E−14	−0·3373E−01	0·2949E−01
−0·5222E−15	−0·9647E−01	−0·3231E+01	−0·4441E−14	0·3348E+00	−0·1861E−01
−0·4309E−15	−0·2393E−01	−0·2528E+01	−0·4099E−14	0·5686E+00	0·6541E−01
−0·2488E−15	−0·4639E−01	−0·1627E+01	−0·2777E−14	0·6105E+00	−0·2546E−01
−0·2022E−15	−0·1297E+00	−0·7074E+00	−0·1741E−14	0·4307E+00	0·1010E+00
0·0000E+00	0·0000E+00	0·0000E+00	0·0000E+00	0·0000E+00	0·0000E+00
(e) *Sixth mode*					
−0·3359E+00	−0·6276E−15	0·8035E−15	0·2759E+01	−0·7050E−15	−0·2365E−15
−0·3193E+00	−0·3801E−15	0·2118E−15	0·2509E+01	−0·6534E−15	−0·2449E−15
−0·3461E+00	−0·2183E−15	−0·4554E−15	0·1914E+01	−0·5234E−15	−0·1726E−15
−0·2825E+00	0·6672E−16	−0·8723E−15	0·9819E+00	−0·2505E−15	−0·1573E−15
−0·3243E+00	0·9038E−16	−0·9353E−15	−0·2054E−01	0·5359E−16	−0·1062E−15
−0·2437E+00	0·2352E−15	−0·5186E−15	−0·1119E+01	0·3289E−15	0·8436E−17
−0·2674E+00	0·1798E−15	0·1650E−15	−0·1930E+01	0·4755E−15	−0·3109E−16
−0·2048E+00	0·1028E−15	0·9492E−15	−0·2594E+01	0·4365E−15	0·8821E−16
−0·1837E+00	0·1079E−15	0·1504E−14	−0·2715E+01	0·2580E−15	0·2450E−16
−0·1597E+00	−0·4032E−16	0·1654E−14	−0·2604E+01	−0·1793E−17	0·1775E−16
−0·8898E−01	0·2545E−16	0·1346E−14	−0·1921E+01	−0·2031E−15	0·3737E−16
−0·9920E−01	0·3107E−16	0·6978E−15	−0·1146E+01	−0·2291E−15	−0·9986E−16
0·0000E+00	0·0000E+00	0·0000E+00	0·0000E+00	0·0000E+00	0·0000E+00